DOSE-BASED EVALUATION OF A PROSTATE BED PROTOCOL

DOSE-BASED EVALUATION OF A PROSTATE BED PROTOCOL

By OLGA M. DONA LEMUS, B.SC.

A Thesis Submitted to the School of Graduate Studies in Partial Fulfillment of the Requirements for the Degree Master of Science

McMaster University MASTER OF SCIENCE (2012) Hamilton, Ontario (Medical Physics and Applied Radiation Sciences)

TITLE: Dose-based Evaluation of a Prostate Bed Protocol AUTHOR: Olga M.Dona Lemus, B.Sc. SUPERVISOR: Professor M. Wierzbicki NUMBER OF PAGES: xi, 75

Abstract

The image-guided radiation therapy (IGRT) protocol used at Juravinski Cancer Center for post-prostatectomy patients involves acquiring a kV cone beam computed tomography (CBCT) image at each fraction and shifting the treatment couch to align surgical clips. This IGRT strategy is promising but its dosimetric impact is unknown, it requires significant resources, and delivers non-negligible doses to normal tissues. The objective of this work is to evaluate this IGRT protocol and investigate possible alternatives.

IGRT delivered dose is reconstructed by deforming the planning CT to the CBCT images acquired at each fraction, computing dose on the deformed images, and inversely transforming the dose back to the original geometry. The treatments of six patients were evaluated under four scenarios: no guidance (Non-IGRT), daily guidance as performed clinically (IGRT), guidance on alternating days (Alt-IGRT), and daily automated guidance (Auto-IGRT). For one patient, the impact of reducing the planning target volume (PTV) margin to five (IGRT-5) and eight (IGRT-8) mm isotropic was also evaluated.

With the standard clinical PTV margin of ten/seven mm, the evaluated alternatives produced similar results. The minimum dose to the CTV was decreased by 1.6±1.0, 1.2±0.7, and 0.8±0.8 Gy for Non-IGRT, Alt-IGRT, and IGRT, respectively. IGRT with manual shifting did not appear to significantly improve the delivered treatment dose compared to Auto-IGRT (difference in CTV minimum dose was 1.2±2.1Gy). Doses to the organs at risk varied but in general, an increased volume of the bladder and rectum received low doses while smaller portions received high doses. The IGRT-5 and -8 analyses showed the same CTV dose can be delivered with significant reduction in normal tissue exposure. Overall, the desired doses are delivered during IGRT although much of this may be attributed to the large PTV margins currently employed clinically.

Acknowledgments

This thesis would not have been possible without the guidance and support of several people who has provided their valuable assistance in the completion of this study.

First and foremost, I would like to express my eternal gratitude to my supervisor Prof. Dr. Marcin Wierzbicki for the continuous support of my research project, for his patience, motivation, enthusiasm, and vast knowledge. Dr. Wierzbicki has been my inspiration as I hurdle all the obstacles in the completion of this study. I could not have imagined having a better supervisor and mentor for this stage of my professional life.

My sincere thanks also enclose Prof. Dr. Diamond and Prof. Dr. Ostapiak, for their valuable comments and suggestions. Their expertise has enriched the results of this study and was fundamental in formulating the final conclusions.

Thank you to the Hamilton Health Sciences and Foundation for providing the funds for this project.

I gratefully acknowledge Prof. Dr. Farrell and Mrs. Fiona Ahlang for answering the million questions I asked during the last two years. Their guidance and support were especially important for me.

I would also want to thank my dear friends and colleagues Tony, Alex, Sahar, Nataliya, Mark, Derek, and Phanishree for their comments, moral support, for the fun we have had and for their friendship.

Last but not least, I would like to thank my wonderful husband, Lazaro, for being patient, supportive and for the unconditional love. I love you so much, and I would not have made it this far without you.

Contents

List of Tables

List of Figures

List of Abbreviations

3D	Three Dimensional
CBCT	Cone Beam Computed Tomography
CT	Computed Tomography
CTV	Clinical Target Volume
DICOM	Digital Imaging and Communications in Medicine
D_{max}	Maximum point dose to an organ or tumor target
DVH	Dose Volume Histogram
EBRT	External Beam Radiation Therapy
RED	Relative Electron Density
GI	Gastrointestinal
GU	Genitourinary
H	Entropy
HDR	High Dose Rate
HU	Hounsfield Units
IGRT	Image Guided Radiation Therapy
IMRT	Intensity Modulated Radiation Therapy
JCC	Juravinski Cancer Center
LDR	Low Dose Rate
MI	Mutual Information
MLC	Multi Leaf Collimator
OBI	On Board Imager
OAR	Organ at Risk
pCT	Planning CT
PSA	Prostate Specific Antigen
PTV	Planning Target Volume
RTOG	Radiation Therapy Oncology Group
ROI	Region of Interest
TLD	Thermo Luminescent Dosimeter
TPS	Treatment Planning System

Chapter I
Introduction

The image-guided radiation therapy (IGRT) protocol currently employed at the Juravinski Cancer Centre (JCC) to treat post-prostatectomy patients requires significant resources and delivers non-negligible imaging doses to normal tissues. The objective of this study is to evaluate this IGRT protocol against two alternative strategies in terms of the dose-volume statistics for target and organs at risk regions. This chapter outlines the main aspects of prostate cancer including incidence rate, relevant anatomy, and typical treatment options. It will particularly focus on intensity-modulated radiation therapy (IMRT) and IGRT and it will describe the current limitations of these techniques. The analysis of these issues will lead to the introduction of the hypothesis and the statement of the thesis objective. Finally, a review of the state of the art will be presented to support the IGRT protocol evaluation method used in this study.

1.1 Prostate Cancer Statistics

Prostate cancer is the most common cancer diagnosed in men in Canada (excluding non-melanoma skin cancer), with 24 600 and 25 500 new cases estimated in 2010 and 2011, respectively (Canadian Cancer Society's Steering Committee, 2010), (Canadian Cancer Society's Steering Committee, 2010). The development of new procedures to deliver radiation therapy and the introduction of prostate-specific antigen (PSA) screening has decreased prostate cancer mortality (Vivek, 2002). Currently, prostate cancer ranks third in term of mortality with 4100 deaths estimated for 2011 (Canadian Cancer Society's Steering Committee, 2010). These statistics are summarized in Table 1.1.

	2010	2011
All Cancers, New Cases	173,800	177,800
Prostate Cancer, New Cases	24,600	25,500
All Cancers, Deaths	76,200	75,000
Prostate Cancer, Deaths	4,300	4,100

Table 1.1. Estimated new cases and deaths for male cancers in Canada in 2010 and 2011[1,2].

1.2 Anatomy of the Male Pelvis

The adult prostate gland is approximately the size of a walnut and has a mass of about 20 g. The prostate is located inferior to the bladder, posterior to the pubic bone, and just anterior to the rectum as shown in Figure 1.1. It comprises muscular and glandular tissues, with ducts opening into the prostatic segment of the urethra. It is divided in three lobes: a center lobe with one lobe on each side.

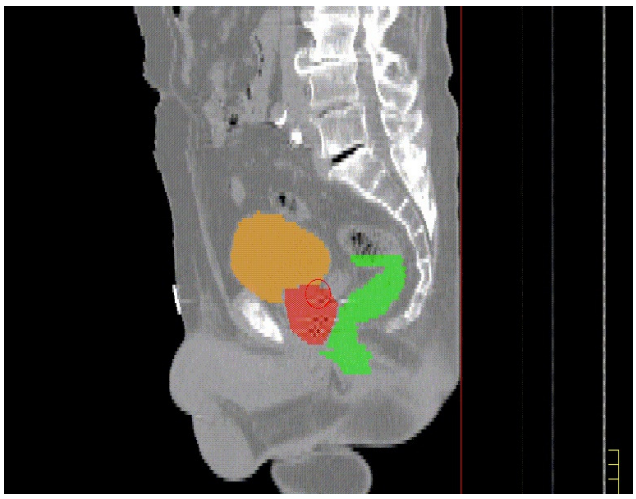

Figure 1.1. Sagittal section of a contoured, male CT image. The red area represents the prostate gland, the green area corresponds to the rectum, and the orange area is the bladder.

The prostate is an exocrine gland in the male reproductive system. Its function is to store and secrete an alkaline fluid, which is one of the components of semen. The function of this fluid is to neutralize the acidity in the vaginal tract, increasing the lifespan of sperm (Jamnicky & Nam, 2009).

1.3 Overview of Prostate Cancer Treatment

Depending on the stage of the disease, a variety of conventional treatment options are available: radical prostatectomy (Boxer *et al.*, 1977), usually with pelvic

lymphadenectomy, hormone therapy (Galbraith & Duchesne, 1997), external-beam radiation therapy (EBRT) (Abdel-Wahab *et al.*, 2012), high dose rate (HDR) and low dose rate (LDR) brachytherapy (Sylvester *et al.*, 2011), chemotherapy (Crawford & Flaig, 2012), and watchful waiting. In addition, several new therapies are being investigated including high-intensity focused ultrasound (El Fegoun, 2011), proton beam radiation therapy (Allen *et al.*, 2012), and ultrasound-guided cryosurgery (Donnelly *et al.*, 2005).

The treatment option of interest in this thesis is EBRT following surgical removal of the prostate. The role of post-prostatectomy radiotherapy is to reduce the risk of recurrence by treating any remaining disease or to provide a salvage option once recurrence is detected. For low risk disease, radiation therapy is limited to the prostatic bed, including areas at high risk of involvement such as the inferior portion of the bladder. This treatment is typically delivered using IMRT as described in the next section. In the case of high risk disease, the entire pelvis is irradiated using large beam apertures to treat the disease as it spreads to the local lymph nodes. This is followed by a boost to the prostate bed volume, typically delivered using IMRT.

1.3.1 Intensity-Modulated Radiation Therapy (IMRT)

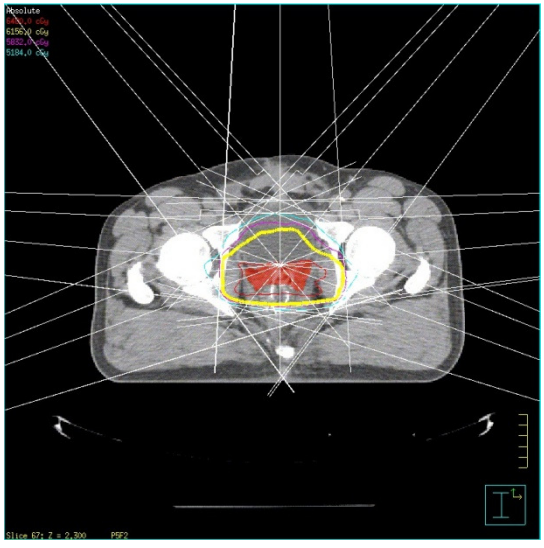

Figure 1.2. Transverse slice of a CT image at the level of the prostate bed showing seven beam angles and the resulting dose distribution.

Delivery of IMRT using a linear accelerator is enabled by the multileaf collimator (MLC), a radiation shield composed of many individual tungsten leaves. These leaves can be positioned dynamically to modulate the intensity of the radiation. In a strategy called Step and Shoot, the gantry rotates and stops at five to nine distinct angles around the patient (see Figure 1.2). At each angle, the MLC leaves are moved to recreate the planned arrangement and a portion

of the total beam time is delivered. The leaves are then repositioned and the second control point, or segment, is delivered. This process is repeated for all planned apertures and the treatment continues with the next gantry angle. Figure 1.3 shows an example MLC configuration used during a post-prostatectomy case.

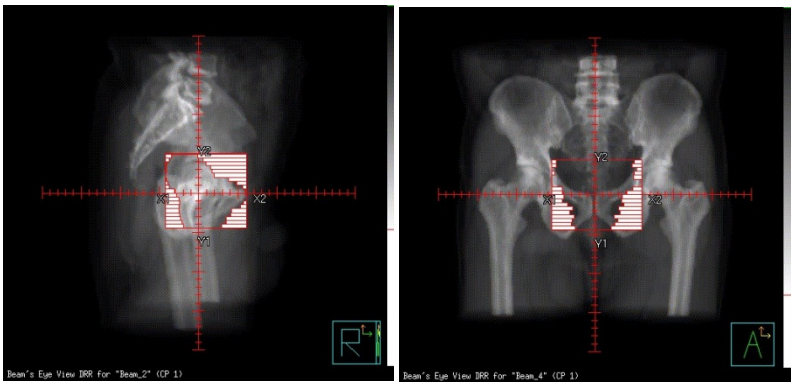

Figure 1.3. MLC configuration for the first control points of the right anterior oblique (left) and the anterior beams (right).

Structure	Volume [%]	D[cGy]
CTV	100	6480
RECTUM	35	6500
RECTUM	55	4000
BLADDER-CTV	50	6500
BLADDER-CTV	70	4000
EACH FEM. HEAD	10	5000

Table 1.2. RTOG 0534 protocol objectives for single phase prostate bed radiation therapy (Pollack, 2011). Other constraints exist but apply to multi-phase treatments (not evaluated in this thesis).

The positions of the MLC and the amounts of radiation delivered by each control point are obtained during treatment planning. Inverse planning is performed by contouring critical organs and the tumour volume in a CT image. The clinical target volume (CTV) contains the gross, palpable tumour (if present) and any areas at an increased risk of subclinical involvement. In prostate bed treatment, the CTV includes the prostatic bed, seminal vesicles, and the bladder neck. The planning target volume (PTV) is a geometric expansion of the CTV. Covering the PTV with the prescribed dose ensures the CTV receives the full dose despite patient set up errors and anatomical motion due to organ filling and breathing. The organs at risk

(OAR) are healthy organs or tissues that affect treatment outcome due to their radiation sensitivity and proximity to the treatment volume. For prostate cancer, the contoured OARs are the bladder, rectum, and femoral heads. Once the anatomy is contoured, the planner places beams to strategically irradiate the volume of interest and defines the appropriate doses to be achieved in the targets and OARs, including their relative importance factors. The prescription dose for prostate bed treatment is typically 64.8 Gy in 36 fractions to 70.2 Gy in 39 fractions. Typically, 95% of the PTV should receive 95% of the prescribed dose. The allowed OARs doses depend on the protocol followed. An example is the Radiation Therapy Oncology Group (RTOG) 0534 clinical trial protocol planning objectives detailed in Table 1.2. Finally, the planner employs the dose computation and optimization engine to find the MLC configuration for each beam that best achieves the user-entered dose criteria (Bortfeld, 2006). An example of a seven beam arrangement and the resulting dose distribution is shown in Figure 1.2.

1.3.2 Image-Guided Radiation Therapy (IGRT)

The dose distribution is based on the assumption that the CTV remains within the PTV despite setup error and organ motion, and that the dose does not change with such errors and motion. A large deviation from the initial geometry could increase the risk of recurrence because the dose delivered to the target volume was insufficient or could result in unnecessary complications due to over irradiation of healthy tissues and organs. One way to address setup errors and normal anatomical variations occurring due to bladder and rectal filling is by increasing the margin between the CTV and the PTV. The disadvantage of a larger PTV is the over irradiation of healthy tissues. A small PTV margin is achievable if the treatment is corrected for variability in setup and patient anatomy at each fraction. This may be achieved by employing the cone beam computed tomography (CBCT), image registration software, and automated couch shifting systems available on some linear accelerators.

At the JCC, a linear accelerator-mounted CBCT system is used to acquire a 3D image of the patient prior to the delivery of each treatment fraction. This image is

compared with the planning CT image and the anatomical difference is assessed. For post-prostatectomy treatments, the goal is to align clearly visible metal clips placed in the patient during surgery. Initial alignment is achieved by automatically registering the two data sets, considering intensity values within a matchbox volume of interest. The matchbox is selected during treatment planning and encompasses as many clips as possible without containing any bony anatomy. Thus, the initial registration aligns the centroid of the clips as observed during planning and treatment. The radiation therapist examines the initial match and performs manual adjustments. Finally, the resulting transformation is used to shift the patient via the treatment couch and the original treatment plan is delivered.

The use of surgical clips as surrogates for the CTV is supported by the work of others. For example, Sandhu *et al*. (Sandhu *et al*., 2008) explored the impact of this image matching strategy on acute radiation toxicity. Prostate bed localization was achieved by aligning the surgical clips observed on kV CBCT with the planning CT image. Most of the patients reported mild grade symptoms. The motion of the prostate bed was measured indicating that margins may be reduced by up to two millimeters from the eight or ten millimeters margin in all directions except five millimeters margin in the posterior used when aligning to bony landmarks alone.

Other IGRT matching structures include bony landmarks and soft tissues surrounding the CTV. Bones are clearly visible in CBCT but bony matching alone does not compensate for the motion and deformation of the CTV due to bladder and rectal filling. Soft tissue matching involves aligning images based directly on the appearance of the soft tissue comprising the CTV and its immediate surroundings. However, current CBCT images acquired on treatment may not exhibit sufficient soft tissue contrast to use this strategy for prostate bed IGRT, although the rectum and bladder often appear with high contrast and may be useful as surrogates for the CTV.

Daily patient positioning based on manual prostate matching versus automatic bone matching for patients imaged using kV CBCT was assessed by Palombarini *et al*.

(Palombarini *et al*., 2012). The total positioning error was calculated as the difference between automatic bone matching followed by manual soft tissue matching and only automatic bone matching. The results showed that the automatic bone matching caused a significant misalignment in the anterior-posterior (AP) axis. This was attributed to the large random motion of the prostate caused by rectal and bladder filling.

1.4 Limitations of IGRT

Although carefully designed, the IGRT protocol used at the JCC has not been investigated in terms of the dose delivered during the entire treatment. Such an analysis is important since IGRT is time consuming, costly, and its use delivers additional, non-negligible doses. Knowledge of how image guidance contributes to the quality of the delivered treatment may lead to improvements of the current IGRT protocol that maximize its benefits.

One drawback of IGRT is the added costs associated with this technique. A potential benefit versus cost analysis for prostate IGRT was performed by Ploquin *et al*. (Ploquin *et al*., 2009). The incremental cost of adding IGRT was calculated using an Activity-Based Costing method, which assigns costs to specific activities such as image acquisition and patient repositioning. They concluded that image guidance used exclusively to reposition the patient costs approximately 2005€/Gy. The improvement in the delivered dose was quantified as the difference in the equivalent uniform doses (EUDs) of the target and OARs for a particular correction protocol minus this difference when no correction is applied. The maximum gain due to IGRT calculated using this metric was estimated at 0.8 Gy.

As with any medical procedure, IGRT also carries some long term risks. Various studies have evaluated the dose associated with CBCT imaging to estimate the risk of developing secondary cancers among long-term survivors. The imaging dose contributed

by kV CBCT during IGRT in prostate cancer patients was investigated by Deng *et al.* (Deng *et al.*, 2012) and Aiping *et al.* (Aiping *et al.*, 2010). They compared Monte Carlo-computed doses delivered using 10-MV IMRT with those delivered by a 125-kV half-fan CBCT scan. The results obtained for kV-CBCT are presented in Table 1.3.

	DOSE (cGy)	
ROI	Deng *et al.* (3 patients)	Aiping *et al.* (1 patient)
Prostate	3.4	1.4
Bladder	4.1	1.7
Rectum	3.8	1.7
Femoral heads	5.7	3.1

Table 1.3 Dose contributed by one kV CBCT image.

They concluded that CBCT dose represented a non-negligible percentage of the IMRT dose. Deng *et al.* also estimated that one CBCT delivers 2.9 cGy to the testes, representing an important increment compared with the 0.7 cGy delivered by IMRT alone. The resulting testicular dose approaches threshold levels for azoospermia. Both studies concluded that the CBCT doses should be either minimized or included in the physician approved dose distribution. The toxicity of CBCT imaging in post-prostatectomy patients was also assessed by Eldredge *et al.* (Eldredge *et al.*, 2011). Dose toxicity was specifically evaluated in the genitourinary (GU) and gastrointestinal (GI) regions and the study included late and acute effects. No association between CBCT and acute GU or GI toxicity was found but the authors conclude that the use of CBCT must be weighed against the increased risk of secondary cancers. Additionally, Kan *et al.* have determined that acquiring daily CBCT images over a standard treatment course may increase the risk of secondary malignancies in a lifetime by approximately 5% since an effective dose up to 1 Sv may be delivered (Kan *et al.*, 2008).

It is also perceived that IGRT may significantly increase treatment time, increasing the logistical strain on the treatment facility. At the JCC, a treatment chart showing the length of the entire treatment, the dates of the planned fractions, the acquisition times for the CBCT images, and the time at which every beam was delivered is available. These data were analyzed for five patients. The time required to achieve image guidance was assumed to be the difference between the CBCT acquisition time and the time at which the first beam was delivered. Over some fractions the patients were required to wait if CBCT detected an inappropriate level of bladder filling or rectal gas. This waiting time was not included the analysis of image guidance time. The mean time used for image guidance is patient specific as shown in Table 1.4. Overall, a total of 2.7 h per complete patient treatment is required. The total treatment time per patient may be estimated by assuming 20 min/fraction × 36 fractions. This gives approximately 12 hours per patient so image guidance takes up about 22.5% of the treatment time. The time spent delivering IGRT at the JCC is considerable and therefore should be justified.

	Patient_01	**Patient_02**	**Patient_04**	**Patient_05**	**Patient_06**
<Time / Fract> [s]	360.0	257.0	281.0	172.0	192.0
St. Dev. [s]	149.2	94.4	101.0	45.9	49.9
Total Time [h]	4.0	3.0	2.7	1.7	1.9

Table 1.4. Mean image guidance time per fraction and the corresponding standard deviation for five patients. The total time image guidance time for the entire treatment is also shown.

1.5 Reduction of the Imaging Doses Associated with IGRT

As discussed in Section 1.4, the additional dose delivered by CBCT during IGRT should not be neglected. Several studies have addressed this issue by including the dose from imaging in the treatment plan, predicting patient shifts based on infrequent imaging, and simply reducing the frequency of imaging.

Parham *et al.* have studied the feasibility of commissioning a commercial treatment planning system (TPS) to calculate the dose resulting from CBCT imaging (Parham *et al*., 2010). The goal was to include the computed CBCT dose in the treatment plan. A RANDO phantom (The Phantom Laboratory, Salem, NY, USA) was used to validate the computation *versus* thermo luminescent dosimeter (TLD) measurements and the differences ranged from 0% to 19 % depending on the anatomical region. It was concluded that computing kV CBCT doses using a TPS produces reasonable results.

Another strategy to reduce imaging dose is to decrease the number of CBCT images taken during treatment. This has the added benefit of reducing resource requirements. Some studies attempted to predict the inter-fraction motion of the bladder, rectum, and prostate, based on several CBCT images acquired at the beginning of treatment. Snir *et al.* for example, evaluated inter-fraction prostate motion of 17 patients undergoing IMRT (Snir *et al*., 2011). In this study, couch shifts were derived using a combination of bone and soft-tissue matching. The mean shift was obtained by considering all fractions and the initial ten fractions. It was concluded that the initial ten imaging sessions were sufficient to predict future shifts without requiring ongoing CBCT imaging. It is important to mention that this strategy requires a larger PTV and therefore, the delivery of higher doses to the OARs.

Whether daily IGRT is required is another issue receiving attention in the literature. Duma *et al*. have quantified the delivered dose to the cervical spinal cord in the treatment of head and neck cancer assuming four IGRT scenarios: image guidance daily, twice per week, once per week, and no guidance (Duma *et al*., 2012). Their results show that the four scenarios produced higher maximum doses than originally planned. Since the daily image guidance method resulted in the smallest dose increase, daily IGRT was recommended for patients planned near spinal cord tolerance, while guidance twice per week was suggested for the remaining patients. The performance of seven IGRT scenarios compared with daily IGRT in the treatment of esophageal cancer was studied by Schiffner *et al*. (Schiffer *et al*., 2012). The effect on the delivered dose for seven IGRT frequency strategies was computed: 0% (non-IGRT), 12% (first three fractions), 20%

(first five fractions), 20% (once per week), 36% (first five fractions and once per week thereafter), 52% (IGRT every other day), 60% (first five fractions and every other day thereafter). The dose volume histograms (DVHs) for heart, lungs, and CTV showed that even for the 60% frequency scenario, significant CTV under dosage and positioning errors occurred. They conclude that daily IGRT is required to treat esophageal cancer. There is a small amount of available data about the optimum IGRT frequency for prostate bed treatment. This could be an interesting area to investigate because the resulting findings may lead to reductions in treatment time and imaging doses.

1.6 Reconstruction of the Delivered Dose in IGRT

When proposing an IGRT protocol it is important to understand its benefits and associated costs. Such information allows the optimization of the technique to maximize its benefit to cost ratio. An appropriate way to evaluate the benefits of IGRT is to determine the dose actually delivered to the patient during the entire treatment. A convenient approach for estimating such a cumulative dose requires the acquisition of a CT or CBCT image at every treatment fraction. The dose is calculated using the acquired image and then registered back to the planning dataset. Once all the fractions have been computed and registered the dose grids are summed and a cumulative dose for the entire treatment is obtained.

Godley *et al.* used this method to estimate the cumulative dose delivered during prostate radiation therapy guided by the CT-on-rails system (Siemens, Munich, Germany) with soft-tissue matching (Godley *et al.*, 2012). They acquired daily CT images (42 in total) for five prostate cancer patients. The daily CT images were imported into the TPS and the dose from the original treatment beams was computed. Each daily CT was deformably registered to the plan CT (pCT) using an in-house deformable registration algorithm. The deformed dose arrays were then summed to obtain the cumulative dose to the patient. A comparison of the cumulative and planned dose distributions showed that

the PTV dose was reduced by up to 3% while the doses to 70% of the bladder and rectum doubled.

The principal imaging system available for prostate bed IGRT at the JCC is CBCT. The dose accumulation technique may be performed by either computing the dose directly using the CBCT images or on a deformed planning CT that represents the patient geometry acquired during CBCT. Either method requires the computation of a deformable transformation that aligns the computed dose grid in the planning CT geometry for summing.

The first approach requires dose computation using CBCT. The principal flaw of this approach arises due to the cone shaped beam used in CBCT imaging. This arrangement simplifies image acquisition but leads to significantly increased scattering compared to fan-beam geometry (Rong *et al*., 2010). The increased beam scattering reduces the accuracy of the measured Hounsfield units (HU) and therefore, affects the accuracy of the conversion from HU to relative electron density (RED). Yang *et al*. evaluated the dose computed using one lung and three pelvic kV CBCT images (Yang *et al*., 2007). The RED vs. HU calibration curve was obtained for the CBCT images and the calibration stability was monitored for an appropriate amount of time. In a static phantom, the dose calculated using the CBCT dataset differed from the dose calculated with the pCT by 1%, while in a motion phantom the discrepancy was 3%, especially in high dose regions. It was concluded that the accuracy of CBCT-based dose calculation is acceptable for low motion regions. CBCT images from 33 patients were compared with the corresponding pCT in a study conducted by Richter *et al* (Richter *et al*., 2008). Four strategies to obtain RED from HU were studied: using a standard RED-HU table, a phantom based table, patient group based (prostate, thorax, head) tables, and patient specific tables. The best results were obtained using the patient group and patient specific tables, with differences of 0.9% between CBCT images and pCT for the pelvic region.

The method used to avoid the issues of calculating dose using a CBCT image employs deformable image registration. In this strategy, the fan-beam CT image used for

treatment planning is aligned with the CBCT image. This deformed CT maintains proper HU, and therefore dose computation accuracy is not affected. However, this approach cannot compensate for extreme anatomical changes such as the replacement of large gas pockets with rectal contents and vice versa. Several researchers have used this strategy to compute the cumulative dose received by the patient during IMRT. Cazoulac *et al*. evaluated the cumulative doses received by a prostate patient during daily IGRT and a head and neck cancer patient with weekly image guidance (Cazoulac *et al*., 2011). The cumulative dose was calculated on the planning CT after deformation to the CBCT dataset. Their approach showed that the dose delivered to rectum, bladder, and parotid exceeded the planned doses.

With either dose computation strategy, image registration is required to appropriately position the resulting dose grids in the planning CT geometry for summing. Cumulative dose computation using deformable image registration has been validated by Niu *et al.* (Niu, T. *et al*., 2012). They produced deformable gel dosimeters to validate the biomechanical model-based deformable registration technique for dose accumulation. The gel dosimeters were treated while compressed by a mechanical device that simulates breathing motion. The mean difference between the gel-measured and computationally accumulated doses was calculated to be 1.5%. This study demonstrates the reliability of the deformable image registration dose accumulation method (Niu, C. *et al*., 2012).

1.7 Image Registration

Image registration is the basic tool required for reconstructing cumulative doses. It is the process of obtaining a transformation that aligns homologous points in a source and target image. An automated image registration algorithm comprises three components: a transformation model describing the allowed modifications of the source image, a similarity metric quantifying the source-to-target image alignment, and an optimization routine that identifies the transformation that maximizes image similarity.

Figure 1.4 shows a simple example of image registration. Considering that image "a" is the source and image "b" is the target we can easily determine that the transformation that aligns "a" onto "b" is a reflection about the "y" axis. This may be written as follows:

$$\begin{bmatrix} x' \\ y' \end{bmatrix} = \begin{bmatrix} -1 & 0 \\ 0 & 1 \end{bmatrix} \begin{bmatrix} x \\ y \end{bmatrix} = \begin{bmatrix} -x \\ y \end{bmatrix}, \qquad \text{(Equation 1)}$$

where (x',y') is the coordinate of the point (x,y) in the source image after the transformation is applied.

a b

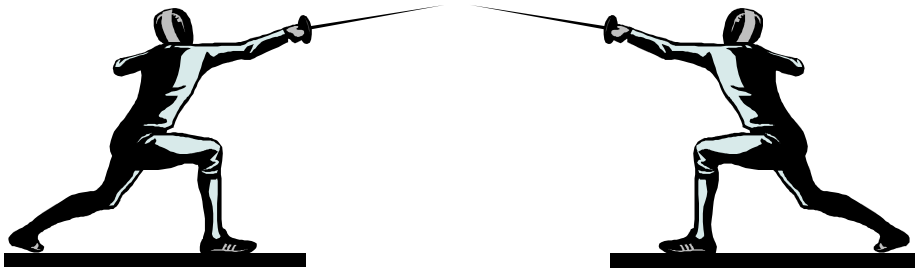

Figure 1.4. Source (a) and target image (b) for the simple registration example.

The situation is slightly more complicated in 3D. For example, obtaining a new point (x', y', z') by transforming (x, y, z) using translations (t_x, t_y, t_z), rotations (θ_x, θ_y, θ_z), and scalings (s_x, s_y, s_z) along the X, Y, and Z axes can be represented as follows:

$$\begin{bmatrix} x' \\ y' \\ z' \\ 1 \end{bmatrix} = \begin{bmatrix} \cos\theta_y\cos\theta_z s_x & -\cos\theta_y\sin\theta_z s_y & \sin\theta_y s_z & t_x \\ (\sin\theta_x\sin\theta_y\cos\theta_z+\cos\theta_x\sin\theta_z)s_x & (-\sin\theta_x\sin\theta_y\sin\theta_z+\cos\theta_x\cos\theta_z)s_y & -\sin\theta_x\cos\theta_y s_z & t_y \\ (-\cos\theta_x\sin\theta_y\cos\theta_z+\sin\theta_x\sin\theta_z)s_x & (\cos\theta_x\sin\theta_y\sin\theta_z+\sin\theta_x\cos\theta_z)s_y & \cos\theta_x\cos\theta_y s_z & t_z \\ 0 & 0 & 0 & 1 \end{bmatrix} \begin{bmatrix} x \\ y \\ z \\ 1 \end{bmatrix}$$

(Equation 2)

Nine degrees of freedom denoted by the above transformation are not sufficient to represent the non-rigid motion occurring in the pelvis due to bladder and rectal filling. One way of representing the required deformable transformation is to create a regular grid of nodes over the source image. At each node, a 3D vector is defined which depicts the

local deformation occurring in this part of the image. Locations between the nodes are deformed by interpolating the vector field. The degrees of freedom enabled by this transformation are defined as three times the number of nodes in the grid. Figure 1.5 shows an example of a vector field describing a deformable transformation.

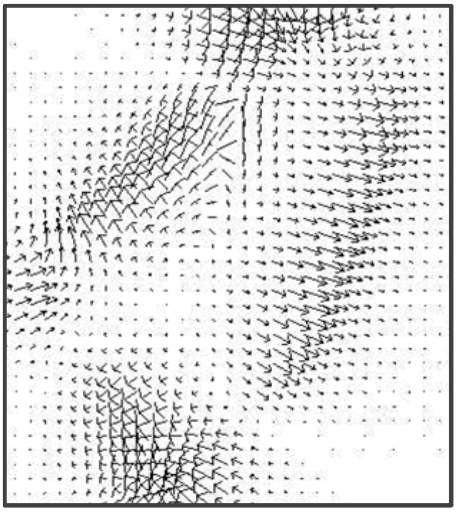

Figure 1.5. Vector field depicting an image deformation transformation.

After determining the transformation model, it is important to define how image alignment will be quantified. Especially interesting are intensity-based similarity metrics since they use the image data directly without requiring the user to identify additional points or geometric structures. An important intensity-based metric used previously to align CBCT and CT images is mutual information (MI). MI is the amount by which the uncertainty about one image decreases when another is known (it is the amount of information contained in one image about the other image). This quantity is computed as follows (Collington *et al*., 1995).

$$\mathrm{MI(Source, Traget)=H(Source)+H(Target)-H(Source,Target)}, \quad \text{(Equation 3)}$$

where H(Source) is the entropy of the source image, H(Target) is the entropy of the target image, and H(Source, Target) is the joint entropy. These quantities may be computed using Shannon's definitions (Shannon, 1948).

$$\mathrm{H(Source)} = -\sum_i \mathrm{P_i ln\, P_i}, \quad \text{(Equation 4)}$$

$$\mathrm{H(Target)} = -\sum_j \mathrm{P_j ln\, P_j}, \quad \text{(Equation 5)}$$

$$\mathrm{H(Source, Target)} = -\sum_j \sum_i \mathrm{P_{i,j} ln\, P_{i,j}}, \quad \text{(Equation 6)}$$

where P_i is the probability that the intensity value i occurs in the source image, P_j is the probability that the intensity value j occurs in the target image, and $P_{i,j}$ is the probability that i and j occur simultaneously in source and target respectively.

The final component of a registration algorithm is the optimizer. This routine identifies the parameters describing the transformation such that the similarity of the source and target images is maximized. One optimization method used widely in image analysis is the Downhill Simplex approach described by Nelder and Meade (Nelder & Meade, 1965). The algorithm constructs an n-dimensional polyhedron with n + 1 vertices, where n is the number of degrees of freedom associated with the transformation model being solved. The similarity metric is evaluated at each of the vertices and depending on the relative values, the polyhedron undergoes geometrical modifications such as reflections, contractions, and expansions. The process continues iteratively until the improvement in similarity metric is below a predefined tolerance.

1.8 Thesis Proposal

The absence of a full dosimetric evaluation of the IGRT protocol currently employed to treat prostate bed at the JCC is the principal motivation for this work. As discussed above, the current protocol relies on automatically registering surgical clips in the CBCT and planning CT images and then performing manual corrections until the clips are visually overlapped. Deviations from planned doses can be relatively large due to variations in patient's anatomy, even if daily image guidance is applied. Thus, it is essential to analyze the dose distribution actually delivered compared with the planned dose. Furthermore, the current IGRT approach is associated with increased costs, time requirements, and imaging doses. This further supports the investigation of actually delivered doses since such an analysis would enable the optimization of the protocol to achieve the best dose distribution and minimize imaging dose, time, and costs. For example, reducing the frequency of image guidance may lead to the delivery of an appropriate dose but reduce these three factors. Finally, a dosimetric analysis would also

enable the study of the impact of PTV size on the coverage of the CTV. Any reduction in margins will decrease doses to the OARs.

The goal of this thesis is to evaluate the cumulative dose delivered by the IGRT protocol currently employed at the JCC. This will provide solid evidence to continue applying the current approach clinically despite the associated time constraints, costs, and risks. Computing the actually delivered dose will also allow the investigation of several modifications of the current protocol. Specifically, this thesis evaluates the dosimetric impact of reduced imaging frequency, decreased PTV margin, and the manual tweaks routinely performed by radiation therapists to improve automatically-derived couch corrections. Such an analysis could support important modifications of the current protocol if the impact on the cumulative dose is determined to be significant.

To perform this analysis, data from the treatments of six post-prostatectomy patients were analyzed. The data for each patient comprise daily acquired CBCT datasets, plan CT datasets, and the treatment history datasheets. Cumulative dose was reconstructed using an image registration-based approach similar to what was outlined in Section 1.6. Dosimetric results were summarized by computing the dose volume histograms (DVH) for the CTV, rectum, bladder, and femoral heads under various IGRT scenarios.

Chapter II
Materials and Methods

The goal of this thesis was to evaluate the post-prostatectomy IGRT protocol used at the JCC. Three additional cumulative dose scenarios were analyzed: no IGRT, IGRT at alternating fractions, and automated IGRT. The dose distributions were calculated using an image registration-based method similar to those introduced in Chapter 1.

2.1 Materials

A portion of this work was performed on a laptop computer running the Ubuntu 10.10 Linux operating system (Canonical Ltd., London, UK). Image processing tasks were completed using python 2.4 (Python Software Foundation, Delaware, USA) scripts that interfaced with a custom version of the Visualization Toolkit (Kitware, Inc., Clifton Park, USA). The majority of the scripts were developed previously although various changes were necessary for this work. A detailed list of the scripts may be found in Appendix 1.

Doses were computed using the Adaptive Convolution technique implemented in the Pinnacle (Phillips NV, Amsterdam, Netherlands) treatment planning system (TPS). The system was also used to obtain the DVHs and to perform treatment planning tasks.

Finally, data from the treatments of six post-prostatectomy patients were used in this analysis. Data for each patient comprised the planning CT image acquired before the therapy and the CBCT images acquired at every fraction. The coordinates of the couch during the acquisition of each CBCT and treatment delivery were obtained from the MOSAIQ record and verify system (Elekta, Stockholm, Sweden) and the CBCT image headers. All data were anonymized to protect patient privacy.

2.2 Cumulative Dose Reconstruction

As discussed in Chapter 1, a convenient method for reconstructing the cumulative dose delivered to the patient during IGRT involves registering CBCT datasets to the planning CT. Dose computation may then be performed directly using the CBCT data or using the deformed versions of the planning image. The latter method was chosen to avoid dosimetric errors resulting from HU inaccuracies in CBCT images. The dose distributions obtained per fraction were multiplied by the total number of fractions and divided by the number of fractions included in the analysis. Finally, the set of corrected doses was inversely transformed back to the planning CT geometry and summed to obtain the cumulative dose. The following sections describe this method in detail.

2.2.1 Image Registration

Several pre-processing steps were required before registering the CBCT and CT images. First, all data were converted to the same format. The Pinnacle image type (P3) was selected because the planning CT image already exists in this format in the TPS. Thus, the DICOM CBCT images were converted to P3 before further analysis. The second step was to align the CBCT image isocenter with the isocenter selected for treatment in the planning CT image. This was achieved by modifying the origin of the CBCT image such that its geometric centre was aligned with the planning isocentre coordinate. The third step was to limit the area of the images considered during image registration to improve accuracy and reduce computation time. Since the region of interest for this study includes the prostate bed, bladder, rectum, and medial aspects of both femoral heads, a registration mask was created with the dimensions shown in Figure 2.1. Another pre-processing step was to correct the difference in voxel size between the CT and CBCT datasets. Since the image similarity computation requires a one-to-one correspondence between source and target image voxels, all data were resampled using tri-linear interpolation to match the CBCT data. Finally, the rectum and bladder in all images were binarized. This was achieved by manually contouring these structures and overriding them with 2047 and 4095 for the bladder and rectum, respectively. This was

necessary because the majority of the motion inside the mask is associated with the bladder and rectum. Furthermore, there is little image contrast between these structures and the surrounding soft tissue. Binarization improves the ability of a deformable image registration algorithm to capture large amplitude motion (Godley *et al.*, 2009). The final images ready for registration are shown in Figure 2.2.

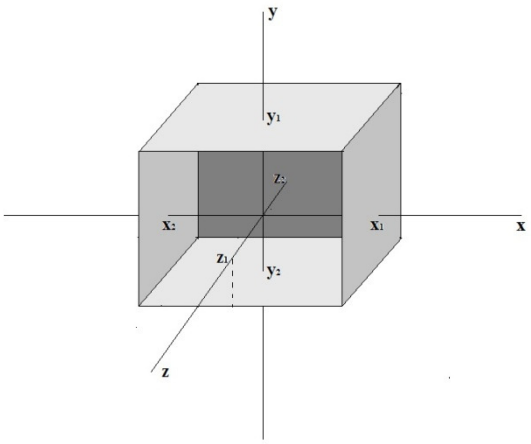

X_1: medial aspect of the left femoral bone.

X_2: medial aspect of the right femoral bone.

Y_1: 1cm anterior to the bladder.

Y_2: 1cm posterior to the rectum.

Z_1: 1cm inferior to the rectum.

Z_2: 1cm superior to the bladder.

Figure 2.1. Mask extents x_1, x_2, y_1, y_2, z_1, z_2. This mask represents the region of interest for the registration method.

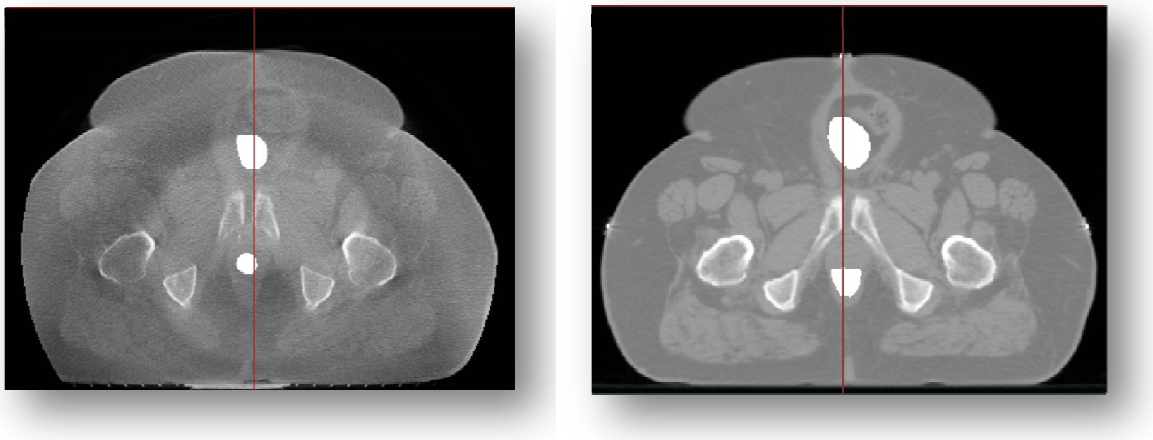

Figure 2.2. Pre-processed CBCT (left) and planning CT (right) images.

Alignment of the CT and CBCT datasets was performed in two steps using previously validated algorithms (Wierzbicki. *et al.*, 2010). The first registration involved the computation of a global transformation that included 3D rotations, translations, and

scalings. The Downhill Simplex optimizer was employed and image similarity was quantified using MI. Since patient setup using tattoos and room lasers provided good initial alignment, constraints were imposed to disallow translations greater than 10 mm, rotations greater than three degrees, and scaling over three percent. This strategy reduced the optimization search space, therefore improving the robustness of the registration algorithm.

The global registration was then refined by computing a deformable transformation, represented using the 3D vector field approach described in Section 1.7. Image similarity was measured using MI and the Downhill Simplex optimizer was employed once again. A trial and error approach was used to select algorithm parameters that resulted in the best image alignment as assessed visually. The final grid spacing parameter defines the resolution of the transformation; minimal grid spacing is ideal but processing time increases considerably for denser vector fields. This parameter is set along with the number of scales the algorithm will consider in its multi-resolution approach. For this study, the scale parameter was set to three and the final grid spacing was 7.5 or 10 mm. This meant that an initial registration was performed with 30 or 40 mm grid spacing (ten iterations), refinements were made once the grid was subdivided into 15 or 20 mm spacing (ten iterations), and fine tuning was performed at 7.5 or 10 mm grid spacing (ten iterations). This multi-resolution approach improves the robustness of the algorithm. The minimum percents parameters define the portion of voxels surrounding a particular vector field node required to be within the mask before that node is included in the registration. This parameter was generally set between 70% and 100%. Alpha is a regularization parameter that restricts the magnitude of the deformation. Its purpose is to prevent extreme deformations unless they are highly favored as quantified by a large increase in the image similarity metric. Values set for this parameter were mostly patient specific and, for some cases, fraction specific. Three alphas were selected for every registration [α_1, α_2, α_3], pertaining to each of the three scales of the multi-resolution optimization approach. Appendix 2 contains the values used for all registrations.

The result of the global and deformable registrations was a combined transformation that aligned the planning CT with the CBCT image. The total transformation was computed for every fraction in each patient and it was applied to the original planning CT images. This process generated a set of new deformed images that represent the patient following setup for every treatment fraction. As discussed in Chapter 1, the deformed images preserve the appropriate HU values. Furthermore, since the field-of-view of CBCT images is restricted, especially for full-fan scans, using the deformed CT images maintains an appropriate external patient contour. These characteristics enable the use of the deformed CT images for dose computation.

Each registration result was validated visually by comparing the transformed planning CT with the CBCT image as shown in Figure 2.4. Figure 2.5 shows the final deformed image for the first fraction of the first patient that was used for the dose distribution calculation in the TPS.

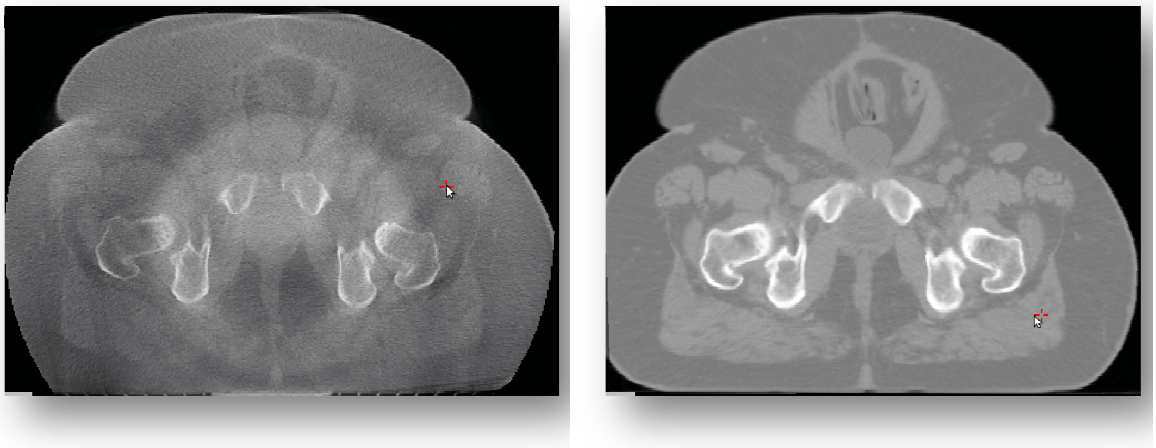

Figure 2.3. Visual validation of the registration process. Transverse slices of the CBCT (left) and transformed planning (right) images.

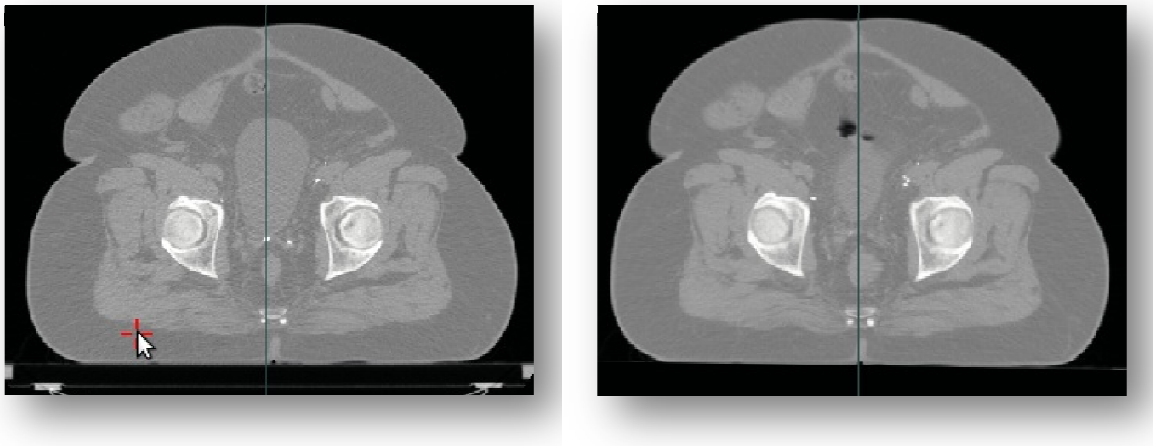

Figure 2.4. Planning CT image (left) and the CT image registered with the CBCT dataset (right).

2.2.2 Registration Limits

Using visual validation, it was established that the image registration algorithm was not effective if the magnitude of the required deformation exceeded approximately three centimeters. This affected deformations due to bladder filling which were different at every fraction as shown in Figure 2.6. In theory, when a patient presents for treatment with a significantly smaller bladder than observed during treatment planning they are asked to drink fluids and return later. In practice, patients may not tolerate the same bladder filling for long periods of time, so radiation therapists may administer treatment despite residual differences. Considering these limitations, only fractions with less than a three cm difference in bladder filling were included in the analysis. Thus, the applicability of this analysis depended on the number of fractions that exceeded the three cm limit. Overall, approximately 15% of images were replaced with other nearby fractions based on this criterion. As a result, the effect of excluding these fractions from the following analyses is likely to be small. Furthermore, with increased experience, radiation therapists are likely to improve the decision making process and more effectively restrict treatment if large bladder filling differences are detected due to concerns over additional bowel dose.

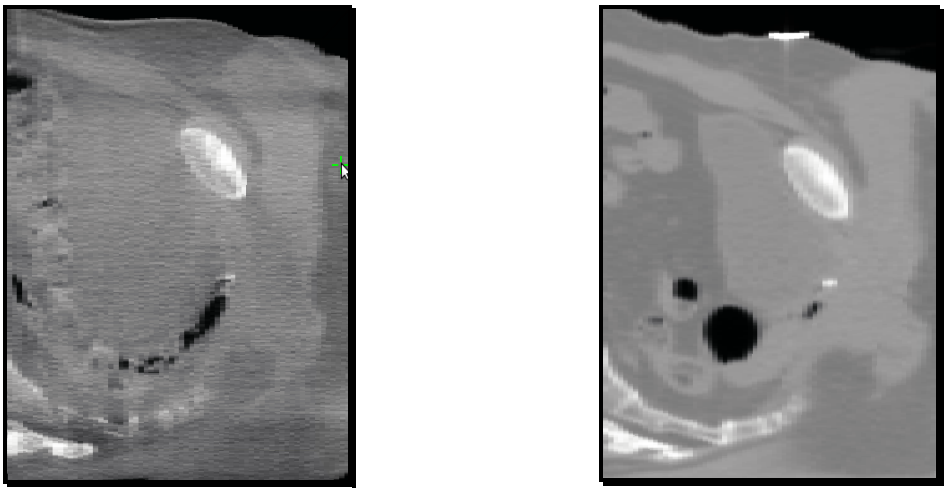

Figure 2.5. Sagittal slice from the CBCT image taken before treatment (left) and the CT image used for planning (right). The difference in bladder filling is approximately three cm.

2.2.3 Dose Computation

The deformed planning CT images for each patient and fraction were imported into the TPS. These data represented the patient geometry following setup only (no image guidance). Treatment beams from the original plan were imported and the dose was computed using the Adaptive Convolve algorithm.

The resulting dose grids were exported and inverse transformed to the original planning CT geometry. This was repeated for all fractions. All fraction dose grids were summed and the total dose grid was imported over the original planning CT image. An example of a cumulative dose grid is shown in Figure 2.7. Finally, the total DVHs for the patient were computed using the regions of interest (ROIs) originally defined for clinical use. The resulting cumulative DVHs represent the dose that would be delivered to each patient if they were treated without any image guidance (i.e. using clinical setup only). These results will be referred to as “Non-IGRT” for the remainder of the thesis.

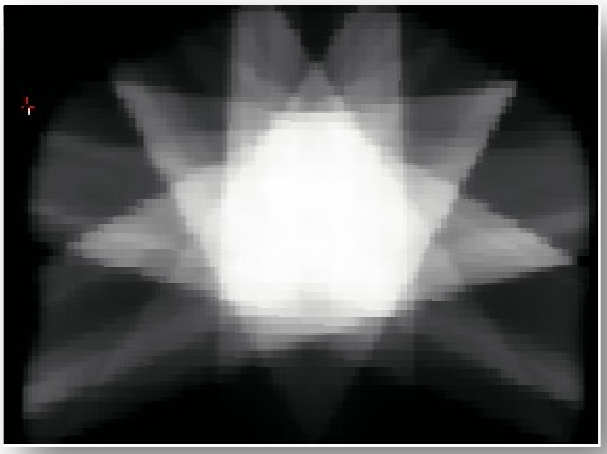

Figure 2.6. Cumulative dose delivered to patient 1.

2.2.4 Determining the Number of Fractions to Analyze

Each of the six patients in this study received 36 treatment fractions, thus the total number of fractions to be evaluated was 216. Among other manual tasks, each of the 216 3D images required contouring to enable the registration process. To avoid this massive undertaking, the impact of representing the entire treatment using a reduced number of fractions was analyzed. Cumulative doses for the six patients were computed by including five and then ten fractions. These fractions typically corresponded to alternating treatments from the first 20 treatments, although nearby replacements were used when the registration limits discussed above were violated. The dose was summed by weighting each fraction by 36/5 or 36/10, depending if five or ten fractions were chosen to represent the entire, 36 fractions treatment. The resulting DVHs were compared to determine the impact of representing treatments using a reduced number of fractions.

The minimum number of patients to be studied to achieve a 95% confidence level in the results was calculated as 22 patients. The allowed margin of error for the CTV was set at 1.8 Gy (dose prescribed at every fraction), and the standard deviation (STD) was set at 4.3 Gy (maximum STD observed during the study). The minimum number of patients was calculated using Equation 7.

$$\epsilon = 1.96\frac{\sigma}{\sqrt{n}} \quad , \qquad \text{(Equation 7)}$$

where ϵ is the margin of error, σ is the STD and n is the minimum number of patients to achieve a 95% confidence level. Due to time limitations, only six patients were analyzed and further work is needed to improve confidence in the results.

2.3 Cumulative Dose Reconstruction for IGRT

When the CBCT datasets were acquired, the coordinates of the couch were recorded in the image headers and in the MOSAIQ patient treatment history. The couch coordinates at the time of irradiation were recorded only in the patient treatment history datasheet.

The shift applied to the patient was computed using the difference between the couch coordinates at CBCT acquisition and the treatment. The shift is the result of performing image guidance during treatment, therefore by shifting the deformed planning CT images obtained in Section 2.2; it is possible to compute the cumulative dose delivered during IGRT.

During the implementation of this method, every shift applied during the treatment was verified. Two tests were performed to validate the shifts recorded in the CBCT datasets. The first test involved applying the recorded shifts to the CBCT image and visually comparing the results with the CT image. This showed whether or not the shifts were applied in the right direction. The second test involved employing the global registration algorithm (translational degrees of freedom only) to automatically register the CT and CBCT images. The theoretical shift, shown in Table 2.2, was compared with the shift obtained when considering the couch coordinates recorded in the CBCT image. This confirmed that the couch coordinates stored in the CBCT image were appropriated in every fraction of the treatment.

Date	Treatment Shifts (mm)			Automated Shift (mm)		
	t_x	t_y	t_z	t_x	t_y	t_z
01/18/11	3	0	2	4	1	1
01/19/11	2	4	4	2	4	2
01/20/11	1	-1	1	1	-1	1
01/24/11	2	-1	0	2	-1	0
01/26/11	3	0	1	4	0	-1
01/31/11	1	0	3	2	0	2
02/03/11	3	3	6	4	4	4
02/07/11	3	0	1	4	0	-1
02/09/11	-4	4	2	-1	6	2
02/11/11	3	0	1	4	0	-1

Table 2.1. Shift coordinates recorded during treatment delivery compared with automatically derived couch shifts for patient 4**.**

Having determined the actual shift applied to the patients, a shift transformation was constructed as shown in Equation 8. This matrix was applied to the deformed CT images to reproduce the patient geometry at every fraction following image guidance. The translation in the x direction (t_x) was determined as the difference between the lateral position of the couch during CBCT acquisition and the lateral coordinates of the couch during treatment. Translations along the y and z axes (t_y, t_z) were computed as the difference in vertical and longitudinal couch positions, respectively.

$$\begin{bmatrix} x' \\ y' \\ z' \\ 1 \end{bmatrix} = \begin{bmatrix} 1 & 0 & 0 & t_x \\ 0 & 1 & 0 & t_y \\ 0 & 0 & 1 & t_z \\ 0 & 0 & 0 & 1 \end{bmatrix} \begin{bmatrix} x \\ y \\ z \\ 1 \end{bmatrix} \qquad \text{(Equation 8)}$$

The resulting IGRT images were imported in to the TPS and the dose was computed. The dose grids for every fraction were inversely transformed back to the original planning CT geometry and summed. The DVHs for the IGRT scenario were finally obtained. These results will be referred to as “IGRT” for the remainder of the thesis.

2.4 IGRT at Alternating Fractions

Reducing the frequency of CBCT imaging to half would significantly reduce imaging dose and the time required to deliver treatment. To evaluate the impact of such a protocol modification, the dose distributions computed as described above were combined. It was assumed that image guidance was employed at alternating fractions, thus, five IGRT and five Non-IGRT dose distributions were summed (alternating between guidance and no guidance). The resulting cumulative dose was used to obtain the "Alt-IGRT" DVHs, and the impact of halving image guidance frequency was evaluated.

2.5 Automated IGRT

The current IGRT protocol employed at the JCC involves the automated registration of the planning CT and CBCT images within a predefined matchbox volume of interest. This initial match is assessed visually and manual corrections may be performed by the radiation therapist. Throughout the process, the goal is to align the surgical clips clearly visible in both datasets. Visual analysis by the therapists is important because it prevents any misalignment produced by the registration software. However, it is difficult to manually improve a 3D registration since it is impossible to fully display such data on a standard monitor and it is difficult to focus on all areas of the image when performing an image matching task. Finally, it is not clear if manual tweaks in the IGRT process translate to any improvements in the actually delivered dose.

This evaluation analyzes the impact of manual couch shift corrections on the final dose distribution. To achieve this, the CT datasets were automatically registered with each of the CBCT images using the same global registration algorithm as described in Section 1.7 with only translational degrees of freedom enabled. The registration mask was modified to be the same as the matchbox used clinically for image matching. This matchbox was defined in the treatment plan as a ROI that contains as many surgical clips as possible while avoiding any bony anatomy. The resulting translational matrix was applied to the deformed CT images, the data were imported into the TPS, and doses computed as already described. The DVHs for "Auto-IGRT" were generated and

compared with the IGRT DVHs to evaluate the impact of manual alignment tweaks on the cumulative dose.

Chapter III
Results and Discussion

This chapter presents the results obtained in the analysis of the six studied patients. Various graphs illustrate the DVHs obtained for the IGRT, Non-IGRT, Alt-IGRT, and Auto-IGRT scenarios. For one patient, the dosimetric impact of reducing PTV margin from the original ten/seven[1] mm to an isotropic five and eight mm was also investigated. Doses obtained under all scenarios were compared with the original plan by visually assessing the DVHs and using the RTOG 0534 objectives presented in Table 1.2.

3.1 Number of Fractions to Analyze

As discussed in Chapter 2, there was a massive amount of data to process in this project. Also, the image registration limit of three centimeters eliminated some fractions from the analysis. Thus, one of the first tasks was to identify a reduced number of fractions that, when used to accumulate dose, would closely approximate the dose delivered during the entire treatment. Figure 3.1 shows the dose accumulation results for the IGRT scenario when including five versus ten treatment fractions. As shown for patient 1, the difference between five and ten fraction DVHs approaches clinical significance. However, the results from the remaining five patients were very similar to the minimal discrepancies observed in Figure 3.1 for patient 2.

[1] Ten mm in all directions except seven mm in the posterior.

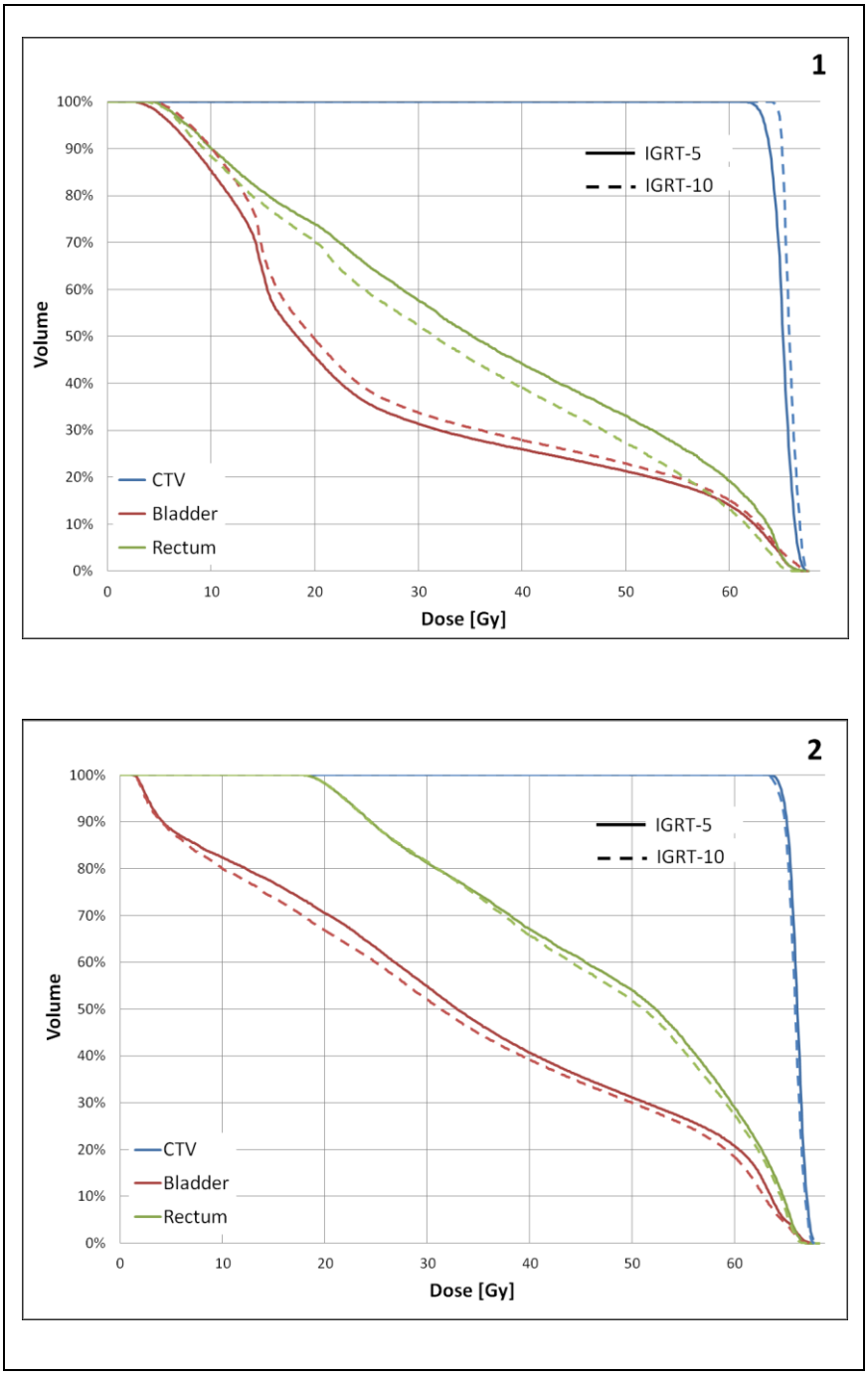

Figure 3.1. Comparison of accumulated DVHs for the IGRT scenario computed using five fractions (solid lines) and ten fractions (dashed lines). Example results are for patient 1 showing the maximum discrepancy and for patient 2 showing the typical discrepancy.

	ΔV (%)		
Patient	CTV($V_{64.8}$)	BLAD(V_{65})	RECT(V_{65})
1	29.7	0.9	2.4
2	3.1	0.6	1.5
3	0.3	1.4	1.6
4	0.4	3.8	1.9
5	1.4	0.8	0.1
6	7.6	0.3	0.0

Table 3.1. Absolute difference in volume between the five and ten fraction DVHs calculated at selected RTOG 0534 dose levels.

Table 3.1 shows the absolute difference in percent volume between the five and ten fraction DVHs evaluated at selected RTOG 0534 dose levels. These data further demonstrate that the dose discrepancy was the largest for patient 1. The highest differences were computed for the CTV due to the steep nature of the DVH around the prescribed dose level. For the OARs, the maximum divergence of 3.8 % was found for the bladder of patient 4. This represents a clinically significant amount, since changes of this magnitude could easily prevent a treatment plan from passing clinical trial or in house DVH criteria.

Ideally all 36 fractions should be included in the analysis due to the unique nature of every image. However, the data presented above shows that for five out of the six studied patients, increasing the number of included fractions from five to ten resulted in a clinically irrelevant change in the computed DVHs. For patient 1, it may be argued that the change in the DVHs is clinical significant. Whether or not more than ten fractions should be included was not studied. However, ten fractions represent a considerable portion of the complete treatment and the impact of including additional fractions is likely to be much lower than that shown in Figure 3.1 and Table 3.1. The potentially modest improvement in accuracy was considered to be not worth the additional manual and automated image processing time. Thus, dose accumulation in this thesis was performed using ten fractions as this was considered to appropriately balance accuracy and time requirements.

3.2 IGRT vs. Plan

The effectiveness of radiation therapy is based on the ability to deliver the prescribed dose. In this section, the cumulative dose resulting from the IGRT scenario was compared to the initial treatment plan. An average result for all patients was calculated to illustrate general trends although the raw DVHs for individual patients are available in Appendix 3.

Figure 3.2 illustrates the mean, the maximum and the minimum plan DVHs calculated for the six patients. The mean curves passed all RTOG 0534 limits except the minimum dose to 55% of the rectum (D55) exceeded the allowed 40 Gy. This would have been considered an acceptable variation since up to 65% of the rectum may receive a minimum of 40 Gy. Individually, most patient DVHs passed the OARs constraints except for patient 4 who failed rectum D55 and the D10 for femurs, and patient 6 who failed rectum D55. It is important to note that passing these limits is not crucial since only patient 3 was actually enrolled in the RTOG 0534 trial.

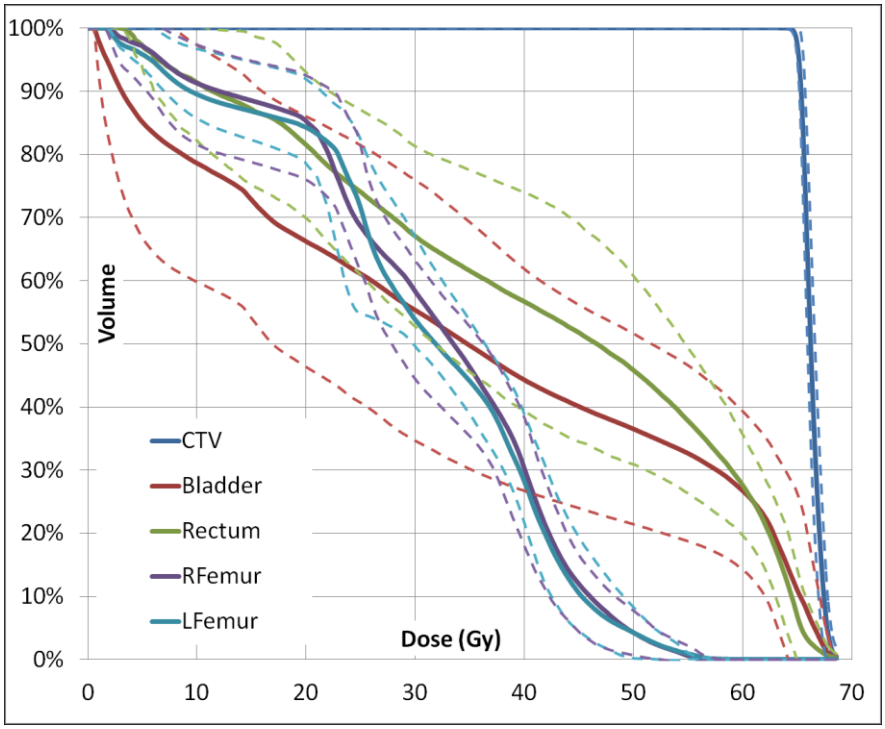

Figure 3.2. Mean plan DVHs calculated for the six patients. The maximum and the minimum deviations from the mean are represented by dotted lines.

Figure 3.3 shows the difference between the mean IGRT and plan DVHs. Overall, an under coverage of the CTV was observed during IGRT. The volume that received 100% of the prescribed dose of 64.8 Gy (V100) was reduced by 4.7±4.5%, V95 was reduced by 0.2±0.4%, V105 decreased by 2.2±2.9%, and the maximum reduction in volume of 15.8 ± 20.0% occurred at 66.3 Gy. These reductions were magnified by the parallel shape of the CTV DVHs around the prescribed dose and the 1D analysis used to obtain the changes in volume. The trends for OARs were patient specific. On average, larger portions of the rectum and bladder received lower doses while smaller volumes were exposed to high doses compared to the plan. This is because the rigid couch shifting technique employed for IGRT does not correct for tissue deformation. The least variability in volumes receiving a particular dose occurred in the femoral heads (volumes within 3% of the plan). This may be attributed to the fact that a low dose gradient was achieved in the bony anatomy during treatment planning. It is acknowledged that these

mean curves only illustrate general trends. Important patient-specific outcomes are presented below.

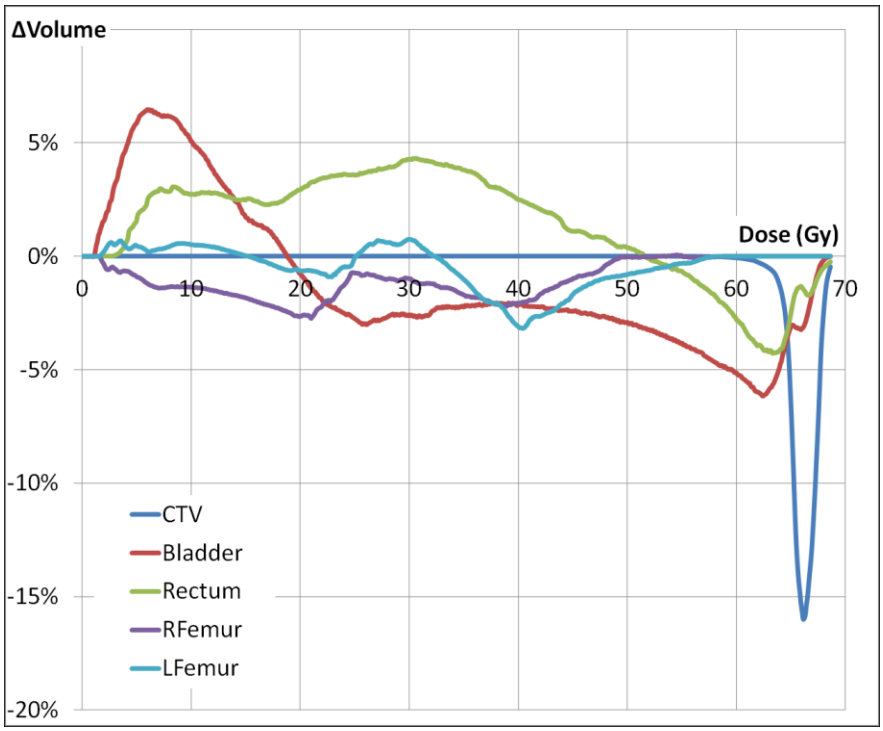

Figure 3.3 Difference between mean IGRT and plan DVHs for the CTV, bladder, rectum, and femoral heads. The standard deviation was approximately 3% for all ROIs.

DVH Quantity	Difference between the IGRT and planned doses (Gy) for Patient							
	1	2	3	4	5	6	F	F_{-3}
CTV(D_{100})	-0.4	-1.5	-10.1	-0.5	0.1	-1.7	1	0
RECT(D_{35})	-2.7	3.4	-12.1	-0.6	0.7	1.0	1	1
RECT(D_{55})	1.0	9.6	-4.7	0.2	5.4	3.8	3	3
BLAD-CTV(D_{50})	1.2	-2.9	-21.1	6.9	4.7	-2.4	2	2
BLAD-CTV(D_{70})	0.9	1.3	-11.7	7.5	1.2	-0.8	1	1
L.FEM. (D_{10})	-1.4	-0.4	-0.6	0.8	1.5	-0.8	0	0
R.FEM. (D_{10})	-1.1	-0.6	-1.0	-0.6	-0.8	-0.7	0	0

Table 3.2 Deviation (Gy) from the plan for IGRT evaluated at the RTOG 0534 DVH limits. The negative values represent an under dose and the positive values represent an over dose. F is the number of failures over all patients and F_{-3} is the number of failures excluding patient 3. The concept of failure is discussed in the text.

Table 3.2 compares the IGRT and planned doses using the RTOG 0534 DVH evaluation criteria. Two failure scores were computed, one included results from all patients (F) and the other excluded results from patient 3 (F_{-3}). The failure score was incremented by one if for a particular patient the CTV was under dosed by 1.8 Gy or an OAR was over dosed by 3 Gy. Patient 3 was excluded (F_{-3}) due to extreme differences in the DVHs that arose due to the following factors. This patient was the only one treated under the RTOG 0534 protocol. Also, his bladder was consistently bigger during the treatment than at planning as seen in the reduction in the bladder doses during IGRT. Furthermore, the rectum contained large amounts of gas during planning and treatment, complicating the accumulation of dose in this ROI. For this patient, rectal gas was overwritten with water density for dose computation in the original plan and in the deformed planning images representing the anatomy during treatment. Despite these efforts, the difference between the plan and the accumulated dose for patient 3 remained much larger than for the other patients, prompting the computation of the two population failure counts F and F_{-3}. The results show that one (F) or zero (F_{-3}) patients failed in terms

of the minimum dose to 100% of the CTV (D100). For the OARs, the F and F_{-3} scores were identical. One patient failed the rectal D35, three failed rectal D55, two failed bladder-ctv D50, and one failed bladder-ctv D70. No patients failed the femoral heads constraint. Due to the challenges faced with patient 3 data and the resulting large DVH differences when compared to the other patients, the F_{-3} results were considered to be a more accurate representation of the dose delivered in the "typical" IGRT scenario.

According to the RTOG 0534 criteria, a typical patient received less dose to the tumour and higher doses to the OARs than planned. The clinical effect of CTV under dosage in prostate radiotherapy was studied by Ash *et al*. (Ash. *et al*., 1994). They determined that a dose reduction of over 10% reduces the five year survival rate by approximately 20%. The effects of under dosing the CTV by approximately two percent level observed in this work were not discussed, although any under dosage probably decreases treatment efficacy. The increased exposure of the bladder and rectum, as demonstrated by the large failure score for these organs, does not compromise the health of the patient since the delivered doses are well within constraints established elsewhere. For example, the RTOG 0126 trial dictates that no more than 15, 25, 35, and 50% of the bladder/rectum should receive 80/75, 75/70, 70/65, and 65/60 Gy, respectively (Michalski, 2010). These OAR limits were easily met for all cases mainly because the prescribed dose in the analyzed prostate bed patients was only 64.8 Gy. However, improvements in the IGRT protocol leading to reduced OAR doses would enable dose escalation, possibility for retreatment, and the delivery of radiotherapy for later stage disease with reduced toxicity.

The results obtained for the typical patient demonstrate the success of the current IGRT approach at the JCC. The target receives the prescribed dose within a small deviation of about two percent, while the OARs are exposed to safe levels of radiation. This is achieved despite the large amount of deformable motion known to occur in the pelvis of a prostate bed patient. However, it is difficult to determine if this success is mainly attributable to IGRT or if it is an effect of the relatively low doses prescribed in

prostate bed and the fact that clinically employed PTV margin overcompensates for residual CTV discrepancies following image guidance. The issues will be examined more closely in the following sections.

3.3 Alt-IGRT vs. IGRT

As discussed in Chapter 1, the reduction of image guidance frequency decreases stochastic (e.g. cancer induction) and deterministic (e.g. azoospermia) effects and reduces the time and resources required for treatment. This section presents the clinical shifts performed for the six patients and the dosimetric impact of Non-IGRT (guidance not employed), Alt-IGRT (guidance at alternating fractions), and IGRT (full guidance). These data will be evaluated to determine if less frequent imaging may be employed to produce similar treatment doses achieved with full IGRT.

Figure 3.4 shows the shifts applied for the six patients during the studied fractions along the lateral (X), vertical (Y), and longitudinal (Z) axes. The overall 3D shift magnitude (R) is also plotted. Table 3.3 shows the mean and standard deviations for shifts performed for all patients along the three axes. The largest mean shifts were recorded in the lateral coordinate for 33% of the patients, in the vertical coordinate for 17% of the patients and in the longitudinal coordinate for 50% of the patients. Therefore, systematic errors occurred most commonly along the longitudinal axis. This may be attributed to the uncertainties in the Z coordinates of the isocentre and ROIs caused by the three mm slice thickness of planning CT data. The largest shifts overall were performed for patient 1 due to the large systematic error in the X direction. It is possible that the relatively large abdomen of this patient shifted the anterior tattoo laterally compared to the planning position. The largest standard deviation also occurred most commonly along the lateral axis, indicating that random errors were dominant in this dimension. Since recorded couch shifts reflect a combination of errors, it was not possible to separate the contribution of setup error and organ motion in this retrospective analysis. An interesting finding overall was that the recorded shifts were easily encompassed within the PTV. Of the 60 analyzed fractions, only two had shifts that exceeded the ten/seven mm PTV

margin employed clinically. The issue of whether the IGRT approach used at the JCC is appropriate given the size of the CTV to PTV expansion is investigated further in Section 3.5.

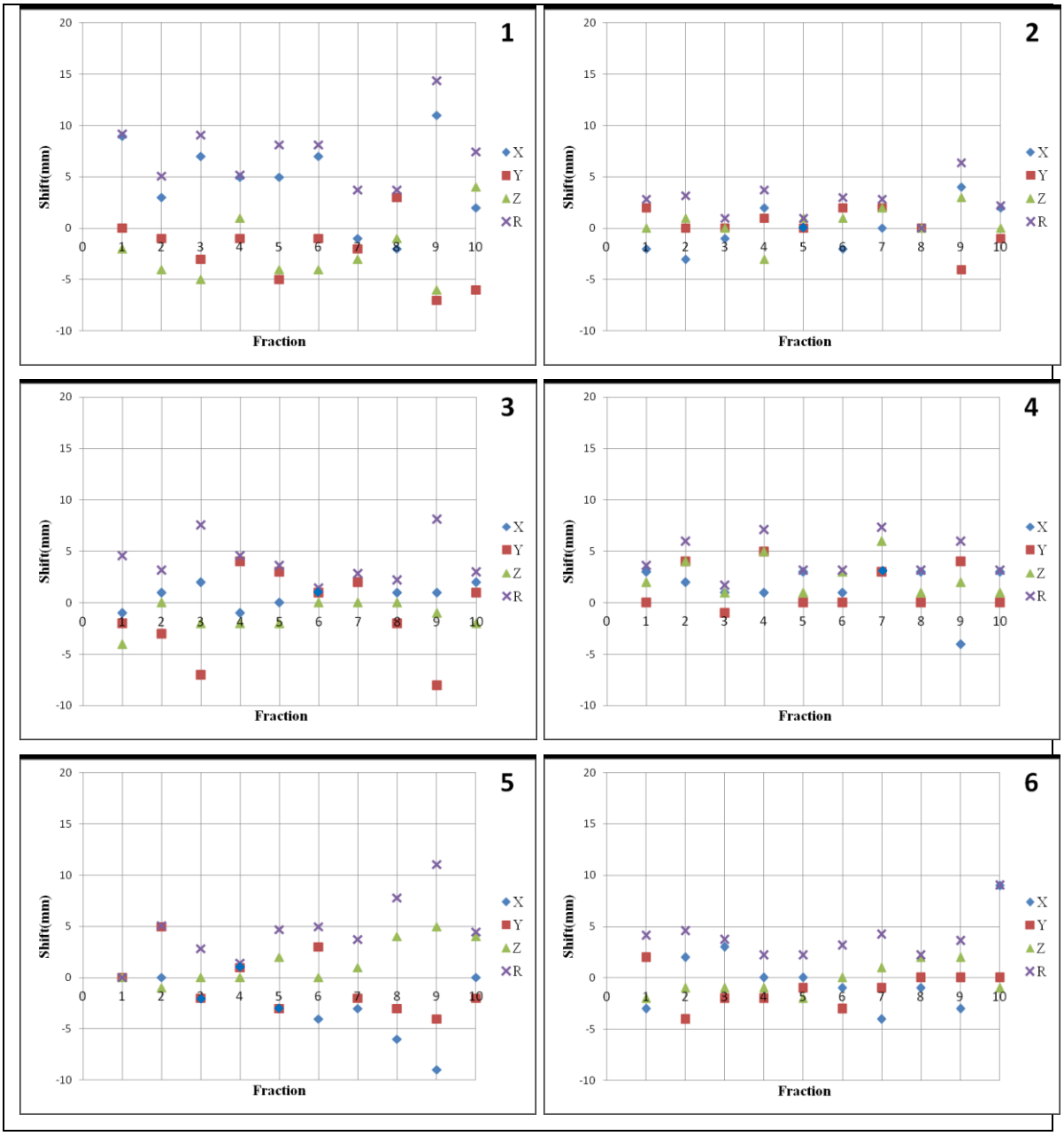

Figure 3.4 Shift applied for each patient at each studied treatment fraction in the lateral (X), vertical (Y), and longitudinal (Z) axes. The total shift is indicated as $R = \sqrt{X^2 + Y^2 + Z^2}$.

	Clinical Couch Shift (mm)			
Patient	**<X>±STD**	**<Y>±STD**	**<Z>±STD**	**<R>±STD**
1	4.6±4.2	-2.3±3.0	-2.4±3.0	7.4±3.2
2	0.0±2.2	0.2±1.8	0.5±1.6	2.6±1.8
3	0.8±1.1	-1.1±4.1	-1.3±1.3	4.1±2.2
4	1.6±2.2	1.5±2.2	2.6±1.8	4.4±2.0
5	-2.6±3.1	-0.7±2.9	1.5±2.1	4.6±3.1
6	0.2±3.8	-1.1±1.7	-0.3±1.5	3.9±2.0

Table 3.3. The mean and standard deviations of clinical shifts performed for each of the six studied patients.

Figure 3.5 shows the difference between the mean DVHs for the Non-IGRT scenario and the plan. As expected, the V95, 100, and 105 for the CTV were reduced by 0.1±0.1, 10.0±11.4, and 1.9±3.7%, respectively. The maximum reduction in volume of 22.7 ± 28.7% occurred at 65.8 Gy. Compared with IGRT, the Non-IGRT DVH demonstrated a larger drop in the target volume receiving a particular dose, although as mentioned above, the V95 remained stable. The difference in volume for the bladder was reduced while the opposite occurred for the rectum. This indicates that patient setup up using tattoos alone placed the isocentre slightly towards the patient's posterior. The femoral heads showed the smallest variability in both scenarios. As shown in Table 3.3, the mean total shift required was 4.5 mm but ignoring these corrections did not seem to affect CTV coverage (V95) or OAR doses. This may be due to the clinically employed PTV margin being too large.

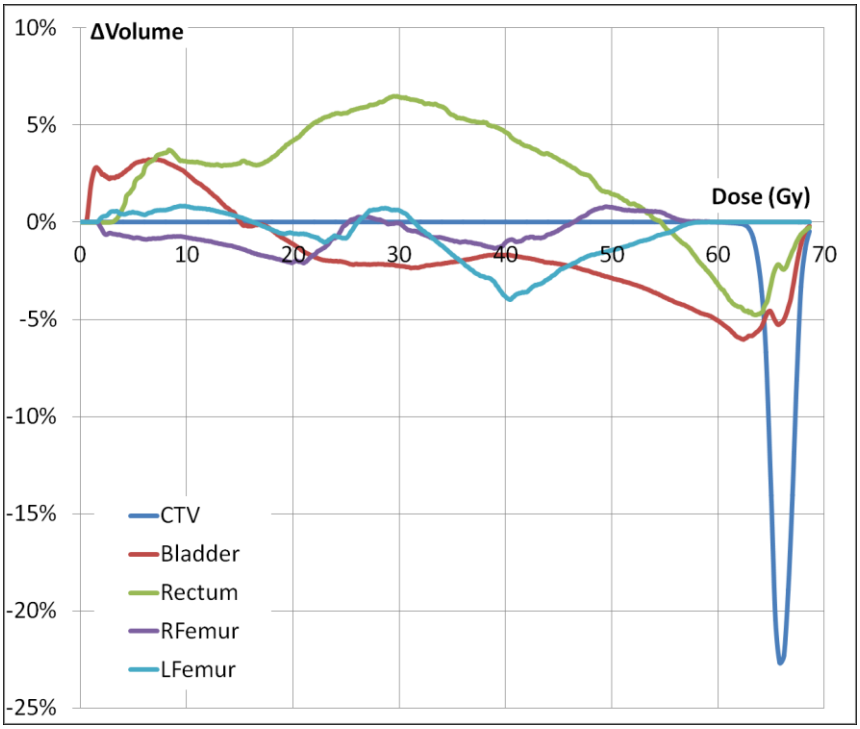

Figure 3.5 Difference between mean Non-IGRT and plan DVHs for the CTV, bladder, rectum, and femoral heads. The standard deviation was approximately 3% for all ROIs.

Table 3.4 compares the Non-IGRT and planned doses using the RTOG 0534 criteria. As in Table 3.2, two patient means were computed: one included all results (F) and the other excluded results from patient 3 (F_{-3}). If the F_{-3} results are taken to be more representative, then two patients failed the CTV coverage criterion, two failed the rectal D35, four failed rectal D55, one failed bladder-ctv D50, and one failed bladder D70-ctv. No patients failed the femur criteria. Once again, these data highlight the mediocre improvement of IGRT over Non-IGRT.

DVH Quantity	Difference between the Non-IGRT and planned doses (Gy) for Patient							
	1	2	3	4	5	6	F	F_{-3}
CTV(D_{100})	-2.7	-1.7	-7.7	-1.7	0.0	-2.1	3	2
RECT(D_{35})	3.3	3.1	-9.9	-2.3	1.0	2.1	2	2
RECT(D_{55})	5.1	9.2	-1.7	-2.0	7.5	6.3	4	4
BLAD-CTV(D_{50})	-1.5	-3.5	-20.0	5.9	2.9	-2.9	1	1
BLAD-CTV(D_{70})	0.9	1.0	-11.1	5.7	1.0	-0.9	1	1
L.FEM. (D_{10})	-0.7	-0.2	-0.5	2.1	-0.1	-0.8	0	0
R.FEM. (D_{10})	-2.8	-0.5	-2.0	-1.1	0.3	-0.7	0	0

Table 3.4 Deviation (Gy) from the plan for Non-IGRT evaluated at the RTOG 0534 DVH limits. The negative values represent an under dose and the positive values represent an over dose. F is the number of failures over all patients and F_{-3} is the number of failures excluding patient 3.

The last scenario evaluated in this section is Alt-IGRT. Figure 3.6 shows the difference between the Alt-IGRT and the plan DVHs. The V95, 100, and 105 for the CTV were reduced by 0.1±0.2, 8.5±8.8, and 2.2±3.2, respectively. The maximum reduction in volume of 22.1±24% occurred at 66.1 Gy. As expected, all DVHs were somewhat in between those presented for IGRT and Non-IGRT, and followed similar trends.

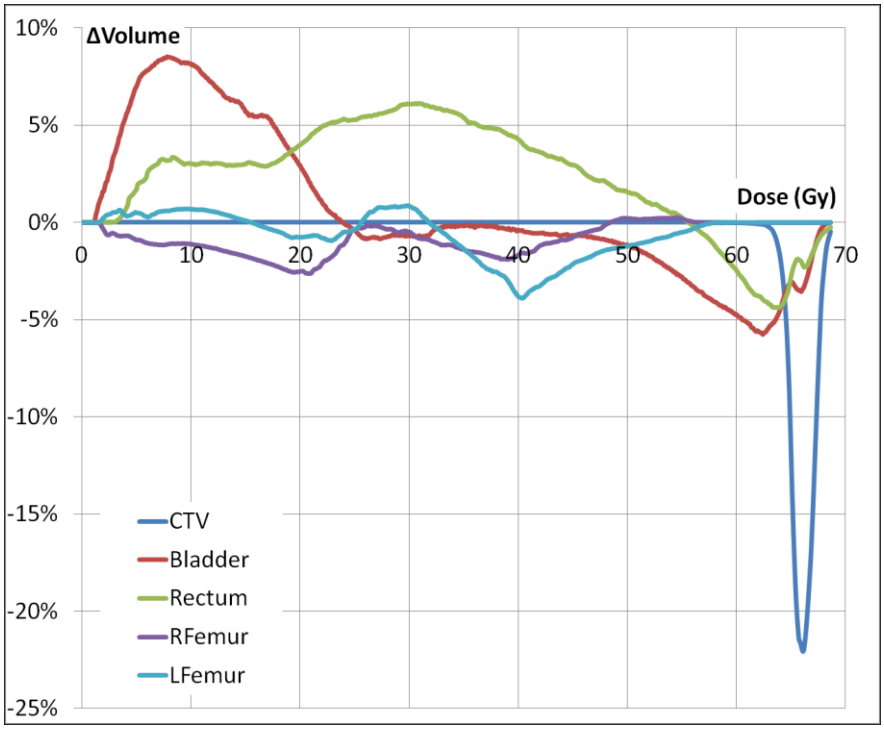

Figure 3.6 Difference between mean Alt-IGRT and plan DVHs for the CTV, bladder, rectum, and femoral heads. The standard deviation was approximately 3% for all ROIs.

Table 3.5 compares the Alt-IGRT and planned doses using the RTOG 0534 criteria. If the F_{-3} results are taken to be more representative, then no patient failed the CTV coverage criterion, one failed rectal D35, four failed rectal D55, two failed bladder-ctv D50, and one failed bladder-ctv D70. No patients failed the femoral head criteria. Since Alt-IGRT is an equal part mixture of IGRT and Non-IGRT, these results fall somewhere in between those already discussed above.

DVH Quantity	Difference between the Alt-IGRT and planned doses (Gy) for Patient							
	1	2	3	4	5	6	F	F_{-3}
CTV(D_{100})	-1.7	-1.6	-8.5	-0.7	-0.1	-1.7	1	0
RECT(D_{35})	1.6	3.3	-10.1	-1.6	2.0	1.3	1	1
RECT(D_{55})	4.2	9.8	-2.0	-0.9	7.4	4.5	4	4
BLAD-CTV(D_{50})	1.6	-3.5	-20.5	6.3	3.4	-2.2	2	2
BLAD-CTV(D_{70})	0.9	0.7	-11.5	6.5	1.1	-0.6	1	1
L.FEM. (D_{10})	-0.9	-0.2	-0.6	1.2	0.3	-1.0	0	0
R.FEM. (D_{10})	-2.4	-0.5	-1.7	-0.9	-0.3	-0.5	0	0

Table 3.5 Deviation (Gy) from the plan for Alt-IGRT evaluated at the RTOG 0534 DVH limits. The negative values represent an under dose and the positive values represent an over dose. F is the number of failures over all patients and F_{-3} is the number of failures excluding patient 3.

All results for IGRT, Alt-IGRT, and Non-IGRT are summarized in Table 3.6. There may be a marginal advantage for IGRT in its ability to cover the CTV, since for all patients, the IGRT D100 was greater than or equal to those obtained using Non-IGRT or Alt-IGRT. Excluding patient 3, the lowest D100 delivered by IGRT was 62.2 Gy (95% of the prescribed dose), indicating that the current margin applied during treatment planning was sufficiently large. However, that margin may in fact be too large since any of the three scenarios are able to provide clinically acceptable CTV coverage. The situation is more complicated in the OARs. All three techniques expose larger volumes of the patient to lower doses and smaller volumes to higher doses. This is due to the inability of the rigid couch shifting technique to compensate for deformable organ motion. The RTOG 0534 limits evaluate doses to relatively large portions of the rectum and bladder ($\geq$ 35%), therefore, it is not surprising that these doses increased compared to the plan. The lowest increase was in the D35 of the rectum, since this was the smallest portion of the OAR evaluated. The dose to the femoral heads remained quite stable probably due to the presence of a low dose gradient in the bony anatomy.

An important limitation of these results is the small sample size and the resulting difficulty in extracting statistically significant conclusions. Furthermore, the analysis is complicated by the large PTV margin employed clinically that seemingly encompasses

much of the motion of the CTV regardless if IGRT is used or not. Additional patients must be studied but these initial results may highlight an important limitation of the approach employed at the JCC. With the current ten/seven mm CTV to PTV expansion, the benefit of IGRT may not be sufficient to warrant the additional imaging doses and time requirements.

DVH Quantity	Failure scores (F_{-3}) for the studied IGRT alternatives		
	Non-IGRT	Alt-IGRT	IGRT
CTV(D_{100})	2	0	0
RECT(D_{35})	2	1	1
RECT(D_{55})	4	4	3
BLAD-CTV(D_{50})	1	2	2
BLAD-CTV(D_{70})	1	1	1
L.FEM. (D_{10})	0	0	0
R.FEM. (D_{10})	0	0	0

Table 3.6 Results for Non-IGRT, Alt-IGRT, and IGRT. Patient 3 was excluded.

A Wilcoxon signed rank test was applied to establish the significance of the obtained results. As expected, the largest difference in delivered doses among the evaluated alternatives was found between IGRT and Non-IGRT. Furthermore, the main objective of treatment is to deliver the dose to the CTV, thus the most important metric to evaluate is the CTV D100. Therefore the statistical test exclusively compared the CTV D100s obtained using Non-IGRT vs. IGRT (data from patient 3 was not included). Performing the Wilcoxon test showed that the D100 delivered by IGRT is significantly better than that delivered by Non-IGRT within a 95% confidence level.

3.4 Auto-IGRT vs. IGRT

This section evaluates the dosimetric consequences of performing manual tweaks on automatically-derived treatment couch shifts. Figure 3.7 shows the difference between the mean Auto-IGRT and IGRT DVHs. Overall, less of the CTV received between 52.0 to 64.8 Gy during Auto-IGRT while more volume received between 64.9 to 68.6 Gy. The V95 and 100 for the CTV were reduced by 0.1±0.3 and 0.0±2.7%, respectively, while V105 increased by 0.0±0.3%. The maximum reduction in volume of 0.4±1.2% occurred at 64.4 Gy and the maximum increment in volume of 2.6±7.8% occurred at 65.8 Gy. Smaller portions of the bladder and the rectum received the same doses with Auto-IGRT compared to IGRT. The femoral heads received approximately the same doses with both methods except in the low dose region where slightly larger volumes were exposed. All of these fluctuations are probably clinically insignificant; therefore, manual tweaks performed during IGRT did not appear to improve the delivered treatment dose. However, it is difficult to attribute this effect to the success of Auto-IGRT since, as discussed previously, the clinically employed PTV margin seems to encompass all CTV motion regardless if image guidance is used.

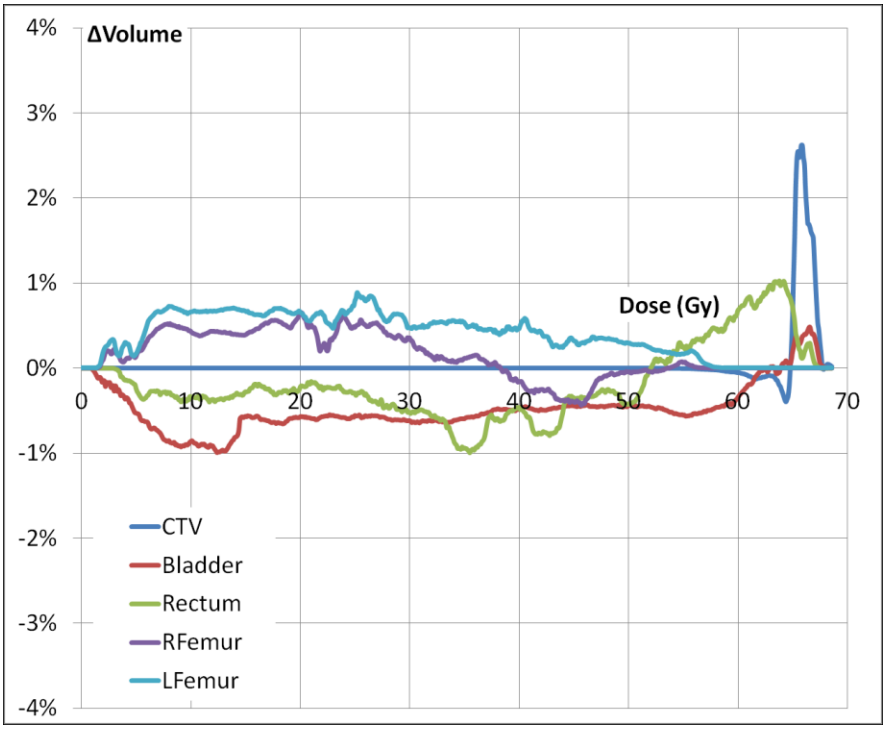

Figure 3.7 Difference between mean Auto-IGRT and IGRT DVHs for the CTV, bladder, rectum, and femoral heads. The standard deviation was approximately 2.4% for all ROIs.

Table 3.7 compares the Auto-IGRT and planned doses using the RTOG 0534 criteria. No patient failed the CTV coverage criterion. One, three, two, and one patients failed the rectal D35, rectal D55, bladder-ctv D50, and bladder-ctv D70, respectively. No patients failed the femoral head objectives. Comparing these results with the ones obtained for IGRT in Table 3.8, identical results for both scenarios have been obtained. This supports the argument that manual couch tweaks do not improve the delivered dose during IGRT. In general, manual tweaking should probably be avoided and the therapists should instead focus on finding cases where large misregistrations have occurred.

DVH Quantity	Difference between Auto-IGRT and planned doses (Gy) for Patient							
	1	2	3	4	5	6	F	F_{-3}
CTV(D_{100})	-0.3	-1.4	-12.3	0.0	0.1	-1.5	1	0
RECT(D_{35})	-5.6	4.2	-15.0	-0.1	0.6	1.0	1	1
RECT(D_{55})	-0.4	11.1	-5.9	0.8	5.1	3.9	3	3
BLAD-CTV(D_{50})	1.8	-3.2	-20.9	5.6	3.7	-3.0	2	2
BLAD-CTV(D_{70})	0.8	0.6	-11.6	6.5	1.1	-1.4	1	1
L.FEM. (D_{10})	-2.7	-0.5	-0.6	0.4	1.4	-0.3	0	0
R.FEM. (D_{10})	-1.1	-0.6	-0.6	-0.2	-0.6	-1.4	0	0

Table 3.7 Deviation (Gy) from the IGRT for Auto-IGRT evaluated at the RTOG 0534 DVH limits. The negative values represent an under dose and the positive values represent an over dose. F is the number of failures over all patients and F_{-3} is the number of failures excluding patient 3.

DVH Quantity	Failure scores for the studied IGRT alternatives (F_{-3})	
	Auto-IGRT	IGRT
CTV(D_{100})	0	0
RECT(D_{35})	1	1
RECT(D_{55})	3	3
BLAD-CTV(D_{50})	2	2
BLAD-CTV(D_{70})	1	1
L.FEM. (D_{10})	0	0
R.FEM. (D_{10})	0	0

Table 3.8 Failure scores for Auto-IGRT and IGRT, excluding patient 3.

3.5 Impact of PTV Margin Reduction

All patients studied in this thesis were treated with a CTV to PTV expansion of ten/seven mm. This margin takes into account linear accelerator inaccuracies, set up motion, and any internal motion during therapy. As shown in Section 3.3, the benefit of IGRT was clinically significant but marginal in magnitude compared to Non-IGRT, indicating that the ten/seven mm margin may be too large. Thus, this section evaluates the

importance of IGRT when the CTV to PTV margin is reduced. Patient 4 was replanned with five and eight mm isotropic expansions of the CTV to obtain the PTV. DVHs representing IGRT were then reconstructed and are shown in Figure 3.8. The changes in the RTOG 0534 criteria from the original plan developed with a ten/seven mm expansion are shown in Table 3.9.

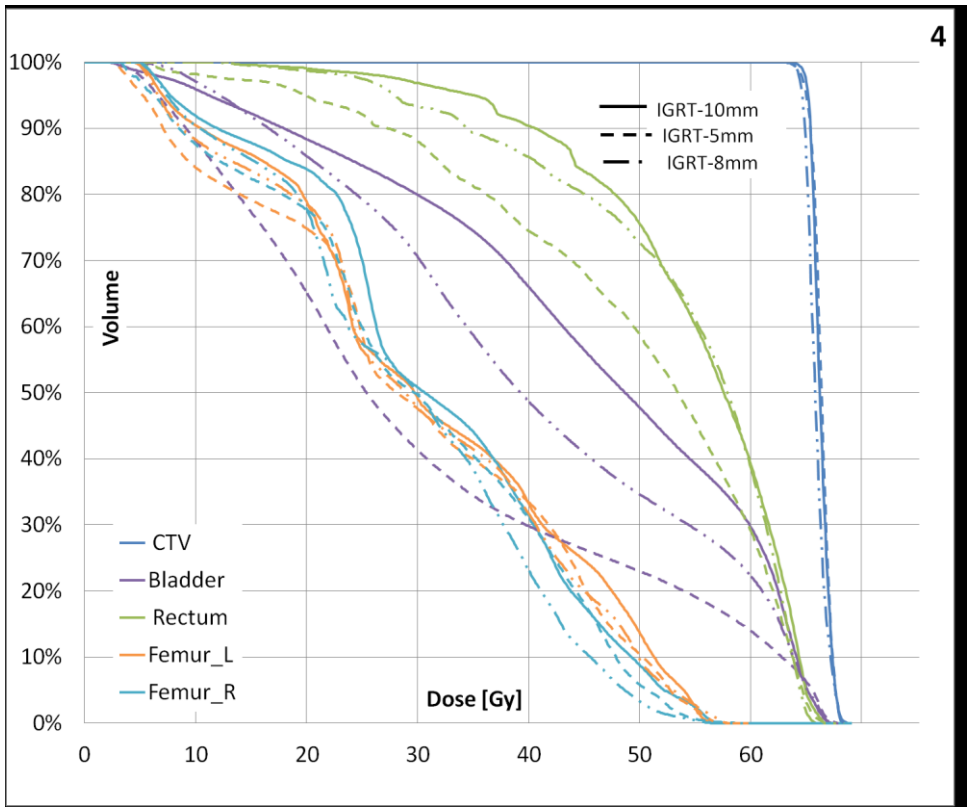

Figure 3.8. Comparison of DVHs reconstructed for IGRT with five mm isotropic PTV margin (dotted lines), IGRT with eight mm isotropic margin (dash dotted lines), and IGRT with the ten/seven mm margin (solid lines) for Patient 4.

DVH Quantity	Difference between the studied IGRT and planned doses (Gy) for patient 4		
	IGRT	IGRT-8	IGRT-5
CTV(D_{100})	-0.5	-0.5	-1.2
RECT(D_{35})	-0.6	-1.2	-3.5
RECT(D_{55})	0.2	0.1	-5.2
BLAD-CTV(D_{50})	6.9	-3.1	-17
BLAD-CTV(D_{70})	7.5	-0.7	-12.8
L.FEM. (D_{10})	0.8	-0.9	-0.6
R.FEM. (D_{10})	-0.6	-4.7	-2.4

Table 3.9. Dose deviation (Gy) from the original plan (ten/seven mm PTV expansion) for IGRT, IGRT-5 (five mm isotropic expansion), and IGRT-8 (eight mm isotropic expansion). These data are for patient 4.

The data in Figure 3.8 and Table 3.9 show that, for patient 4, the optimal PTV margin would be five mm. Such a small expansion would result in an under dosage of the CTV by 1.2 Gy (~ 2% of the prescribed dose), but would provide excellent sparing of the OARs. The improvement in the CTV to OAR dose ratio was the most important in the bladder because the original plan was developed with a 10 mm anterior expansion. Rectal dose was reduced only slightly since the original plan was developed with a seven mm posterior expansion.

This single-patient analysis creates some concern over the optimality of the IGRT approach currently used at the JCC. As shown in Section 3.3, IGRT with a ten/seven mm margin provided only a small benefit compared to Non-IGRT. In this section, it was shown that the same IGRT approach with an eight mm planning margin would result in the delivery of the prescribed dose to the CTV while significantly reducing the dose to the OARs while a five mm margin would provide further improvements, enabling dose escalation or retreatment of recurrent disease with reduced toxicity. Additional patients need to be analyzed to provide statistically significant evidence for reducing treatment margins.

Chapter IV
Conclusions

4.1 Patient Specific Conclusions

Various patient-specific results were obtained during the study of different IGRT approaches. While some alternatives have been found successful for one patient, they may not be the right solution for another. The human body is a very complex system and every patient is different. In this section we will show some patient specific conclusions that will lead to the general conclusion of this thesis.

4.1.1 Patient 1

Table 4.1 shows the results generated for this patient. Over the four alternatives evaluated, the best outcome was obtained for the Auto-IGRT. Auto-IGRT achieves the best CTV coverage while keeping the doses to the OAR under the recommended limits.

Difference between studied alternatives and planned doses (Gy) for patient 1

DVH Quantity	Non- IGRT	IGRT	Alt-IGRT	Auto-IGRT
CTV(D_{100})	-2.7	-0.4	-1.7	-0.3
RECT(D_{35})	3.3	-2.7	1.6	-5.6
RECT(D_{55})	5.1	1.0	4.2	-0.4
BLAD-CTV(D_{50})	-1.5	1.2	1.6	1.8
BLAD-CTV(D_{70})	0.9	0.9	0.9	0.8
L.FEM. (D_{10})	-0.7	-1.4	-0.9	-2.7
R.FEM. (D_{10})	-2.8	-1.1	-2.4	-1.1

Table 4.1. Deviation from the Plan for Non-IGRT, IGRT, Alt-IGRT and Auto-IGRT for patient 1.

4.1.2 Patient 2

As explained before, the bladder of Patient 2 was consistently smaller during treatment and it was very difficult to obtain sufficient CBCT datasets on which image registration was achieved with confidence. Table 4.2 shows that all the evaluated methods produced similar results. While IGRT and Auto-IGRT achieved the best CTV coverage; the doses delivered by Non-IGRT and Alt-IGRT were reduced by merely 0.1 and 0.2 Gy, respectively. In addition, the Non-IGRT alternative delivered smaller doses to the OARs. For this patient, Non-IGRT would produce sufficient CTV coverage while decreasing the dose toxicity, time, and resources during treatment.

Difference between studied alternatives and planned doses (Gy) for patient 2

DVH Quantity	Non- IGRT	IGRT	Alt-IGRT	Auto-IGRT
CTV(D_{100})	-1.7	-1.5	-1.6	-1.4
RECT(D_{35})	3.1	3.4	3.3	4.2
RECT(D_{55})	9.2	9.6	9.8	11.1
BLAD-CTV(D_{50})	-3.5	-2.9	-3.5	-3.2
BLAD-CTV(D_{70})	1.0	1.3	0.7	0.6
L.FEM. (D_{10})	-0.2	-0.4	-0.2	-0.5
R.FEM. (D_{10})	-0.5	-0.6	-0.5	-0.6

Table 4.2. Deviation from the Plan for Non-IGRT, IGRT, Alt-IGRT and Auto-IGRT for patient 2.

4.1.3 Patient 3

Data from patient 3 were not included in the general conclusions due to the high deviation in the results compared with the other patients. This patient was planned using the RTOG protocol while the other five were planned following an in-house approach. Furthermore, when computing the time required for IGRT, the average time between CBCT image acquisition and treatment for this patient was approximately three hours. This highlights the difficulties therapists had in positioning him for treatment. The

registration itself for this patient was challenging due to the large portions of gas inside of the rectum and the extra large size of the bladder during the treatment.

Table 4.3 contains the results for this patient after the evaluation of the four different alternatives. None of the alternatives accomplished acceptable CTV coverage. The CTV D100 was reduced from the plan by 7.7 to 12.3 Gy. The best CTV coverage was obtained for Non-IGRT and Alt-IGRT. The OARs received less dosage for all the studied alternatives. Patient 3 requires further analysis to determine the causes of these large discrepancies.

Difference between studied alternatives and planned doses (Gy) for patient 3

DVH Quantity	Non- IGRT	IGRT	Alt-IGRT	Auto-IGRT
CTV(D_{100})	-7.7	-10.1	-8.5	-12.3
RECT(D_{35})	-9.9	-12.1	-10.1	-15.0
RECT(D_{55})	-1.7	-4.7	-2.0	-5.9
BLAD-CTV(D_{50})	-20.0	-21.1	-20.5	-20.9
BLAD-CTV(D_{70})	-11.1	-11.7	-11.5	-11.6
L.FEM. (D_{10})	-0.5	-0.6	-0.6	-0.6
R.FEM. (D_{10})	-2.0	-1.0	-1.7	-0.6

Table 4.3. Deviation from the Plan for Non-IGRT, IGRT, Alt-IGRT and Auto-IGRT for patient 3.

4.1.4 Patient 4

Patient 4 had a very consistent geometry during treatment, making him suitable for investigating the effect of reducing the CTV to PTV expansion. For this patient, six scenarios were evaluated: Non-IGRT, IGRT, Alt-IGRT, Auto-IGRT, IGRT with a five mm isotropic PTV margin, and IGRT with an eight mm isotropic PTV margin. The results of these analyses are summarized in Table 4.4.

All the alternatives studied generated similar results. The Auto-IGRT scenario produced the best CTV coverage but Alt-IGRT deviated from this result by only one

percent of the prescribed dose. For the margin analysis, the planned dose was best reproduced using IGRT-8. However, the five mm margin showed superior sparing of OARs with only a slight reduction of the dose to the CTV. The reduction of PTV margin is a promising alternative as it maximizes the benefit of IGRT.

Difference between studied alternatives and planned doses (Gy) for patient 4						
DVH Quantity	Non-IGRT	IGRT	Alt-IGRT	Auto-IGRT	IGRT -5	IGRT -8
CTV(D_{100})	-1.7	-0.5	-0.7	0.0	-1.2	-0.5
RECT(D_{35})	-2.3	-0.6	-1.6	-0.1	-3.5	-1.2
RECT(D_{55})	-2.0	0.2	-0.9	0.8	-5.2	0.1
BLAD-CTV(D_{50})	5.9	6.9	6.3	5.6	-17.0	-3.1
BLAD-CTV(D_{70})	5.7	7.5	6.5	6.5	-12.8	-0.7
L.FEM. (D_{10})	2.1	0.8	1.2	0.4	-0.6	-0.9
R.FEM. (D_{10})	-1.1	-0.6	-0.9	-0.2	-2.4	-4.7

Table 4.4. Deviation from the Plan for Non-IGRT, IGRT, Alt-IGRT and Auto-IGRT for patient 4.

4.1.5 Patient 5

As shown in Table 4.5, this patient was extremely stable during radiation therapy since none of the studied alternatives differed from IGRT.

Difference between studied alternatives and Plan doses (Gy) for patient 5				
DVH Quantity	Non-IGRT	IGRT	Alt-IGRT	Auto-IGRT
CTV(D_{100})	0.0	0.1	-0.1	0.1
RECT(D_{35})	1.0	0.7	2.0	0.6
RECT(D_{55})	7.5	5.4	7.4	5.1
BLAD-CTV(D_{50})	2.9	4.7	3.4	3.7
BLAD-CTV(D_{70})	1.0	1.2	1.1	1.1
L.FEM. (D_{10})	-0.1	1.5	0.3	1.4
R.FEM. (D_{10})	0.3	-0.8	-0.3	-0.6

Table 4.5. Deviation from the Plan for Non-IGRT, IGRT, Alt-IGRT and Auto-IGRT for patient 5.

4.1.6 Patient 6

As shown in Table 4.6, all alternatives studied for this patient resulted in reduced CTV coverage. The Auto-IGRT strategy produced the best CTV coverage while reducing the doses to the OARs.

Difference between studied alternatives and planned doses (Gy) for patient 6				
DVH Quantity	Non- IGRT	IGRT	Alt-IGRT	Auto-IGRT
CTV(D_{100})	-2.1	-1.7	-1.7	-1.5
RECT(D_{35})	2.1	1.0	1.3	1.0
RECT(D_{55})	6.3	3.8	4.5	3.9
BLAD-CTV(D_{50})	-2.9	-2.4	-2.2	-3.0
BLAD-CTV(D_{70})	-0.9	-0.8	-0.6	-1.4
L.FEM. (D_{10})	-0.8	-0.8	-1.0	-0.3
R.FEM. (D_{10})	-0.7	-0.7	-0.5	-1.4

Table 4.6. Deviation from the Plan for Non-IGRT, IGRT, Alt-IGRT and Auto-IGRT for patient 6.

4.2 General Conclusions

It has been very difficult during this study to find a method that produces the best solution for all patients. For example, while Alt-IGRT was sufficient for some patients, it was not the best option for others.

Drawing conclusions from these data has been difficult due to three reasons. First, the population size was small considering the amount of patients annually treated at JCC. One patient was excluded due to large deviation in the results compared with the rest of the sample. The remaining population is too small to conclude that the difference between the evaluated IGRT strategies is statistically significant. An exception to this was the difference between IGRT and Non-IGRT in terms of CTV coverage (determined to be statistically significant).

The second problem was that the PTV margin was so large that minimum CTV dose was reduced by up to 2.5% even when no image guidance was employed. The

results obtained for the studied alternatives were very similar, making it hard to identify the best general solution for all the patients. The large PTV margin may result in a waste of the IGRT potential.

Given these limitations a future study is recommended. The same approach should be used although data from more patients must be analyzed. Planning for this study should be performed with a reduced margin (eight mm isotropic as an example). Three of the analyzed scenarios should be compared: IGRT, Non-IGRT, and Auto-IGRT. In addition, instead of investigating Alt-IGRT, a technique for reducing imaging frequency by predicting prostate bed motion should be developed and investigated. It is expected that with reduced PTV margin, the dose delivered by IGRT would be superior to Non-IGRT, while Auto-IGRT and the reduced imaging IGRT approach would produce clinically acceptable results. This study would provide the evidence necessary to alter the protocol employed at the JCC and result in improvements in the utilization of imaging dose and resources.

BIBLIOGRAPHY

Abdel-Wahab, M., Mahmoud, O., Merrick, G. *et al*. (2012). ACR Appropriateness Criteria. External-Beam Radiation Therapy Treatment Planning for Clinically Localized Prostate Cancer. Journal of the American College of Radiology, 9(4), 233-8.

Aiping, D., Jianwei, G., Alexei, V. *et al*. (2010). Monte Carlo calculation of imaging doses from diagnostic multidetector CT and kilovoltage cone-beam CT as part of prostate cancer treatment plans. Medical Physics, 37(12), 6199-204. doi:10.1118/1.3512791.

Allen, A. M., Pawlicki, T., Dong, L. *et al*. (2012) .An evidence based review of proton beam therapy: The report of ASTRO's emerging technology committee. Radiotherapy and Oncology, 103(1), 8-11.

Ash, D. and Bates, T. (1994). Report on the clinical effects of inadvertent radiation underdosage in 1045 patients. Clinical Oncology, 6 (4), 214-226.

Bortfeld, T. (2006). IMRT: A review and preview. Physics in Medicine and Biology, 51(13), R363-R379.

Boxer, R. J., Kaufman, J. J., Goodwin, W. E. (1977). Radical prostatectomy for carcinoma of the prostate: 1951-1976. A review of 329 patients. The Journal of Urology, 117(2), 208-13.

Canadian Cancer Society's Steering Committee. (2010, April). Canadian cancer statistic 2010. Canadian Cancer Society, ISSN 0835-2976.

Canadian Cancer Society's Steering Committee.(2011, May) Canadian cancer statistic 2011. Canadian Cancer Society, ISSN 0835-2976.

Cazoulat, G., Lesaunier, M., Simon, A. *et al*. (2011). From image-guided radiotherapy to dose-guided radiotherapy. Cancer Radiotherapy, 15(8),691-8.

Collington, A., Maes, F., Delaere, D. *et al.* (1995). Automated multi-modality image registration based on information theory. Information Processing in Medical Imaging, 263- 274.

Crawford, E. D, Flaig, T. W. (2012). Optimizing outcomes of advanced prostate cancer: drug sequencing and novel therapeutic approaches. Oncology (Williston Park, N. Y.), 6(1),70-7.

Deng, J., Chen, Z., Yu, J. *et al.* (2012). Testicular doses in image-guided radiotherapy of prostate cancer. International Journal of Radiation Oncology, Biology and Physics, 82(1), 39-47.

Donnelly, B. J., Saliken, J. C., Ernst, D. S. *et al*. (2005). Role of transrectal ultrasound guided salvage cryosurgery for recurrent prostate carcinoma after radiotherapy. Prostate Cancer and Prostatic Diseases, 8(3), 235-42.

Duma, M. N., Kampfer, S., Schuster, T. *et al*. (2012). Do We Need Daily Image-Guided Radiotherapy by Megavoltage Computed Tomography in Head and Neck Helical Tomotherapy? The Actual Delivered Dose to the Spinal Cord. International Journal of Radiation Oncology, Biology and Physics. [Epub ahead of print].

El Fegoun, A. B., Barret, E., Prapotnich, D. *et al*. (2011). Focal therapy with high-intensity focused ultrasound for prostate cancer in the elderly. A feasibility study with 10 years follow-up. International Brazilian Journal of Urology, 37(2), 213–9.

Eldredge, H. B., Studenski, M., Keith, S. W., *et al*. (2011). Post-prostatectomy image-guided radiation therapy: Evaluation of toxicity and inter-fraction variation using online cone-beam CT. Journal of Medical Imaging and Radiation Oncology, 55(5), 507-15. doi: 10.1111/j.1754-9485.2011.02305.x.

Galbraith, S. M., Duchesne, G. M. (1997, April). Androgens and Prostate Cancer: Biology, Pathology and Hormonal Therapy. European Journal of Cancer, 33(4), 545-54.

Godley, A., Ahunbay, E., Peng, C. *et al*. (2012). Accumulating daily-varied dose distributions of prostate radiation therapy with soft-tissue–based kV CT guidance. Journal of applied clinical medical physics, 13(3), 3859. doi: 10.1120/jacmp.v13i3.3859.

Godley, A., Ahunbay, E., Peng, Ch. *et al*. (2009). Automated registration of large deformations for adaptive radiation therapy of prostate cancer. Medical Physics, 36, 1433. doi:10.1118/1.3095777.

Jamnicky, L., Nam, R., & Ebooks Corporation. (2009). The complete Canadian guide to prostate cancer. Hoboken: John Wiley & Sons, Inc.

Kan, M.W., Leung, L.H., Wong, W. *et al*. (2008).Radiation dose from cone beam computed tomography for image-guided radiation therapy. International Journal of Radiation Oncology, Biology and Physics, 70(1), 272–279.

Michalski, J. (2010). RTOG 0534 protocol. Radiation Therapy Oncology Group clinical trials. Retrieved from http://www.rtog.org/ClinicalTrials/ProtocolTable/StudyDetails.aspx?study=0

Nelder, J. A. and Meade, R. (1965). A simplex method for function minimization. Computer Journal, 7, 308-313.

Niu, C. J., Foltz, W. D., Velec, M. *et al*. (2012). A novel technique to enable experimental validation of deformable dose accumulation. Medical Physics, 39(2), 765-76.

Niu, T., Al-Basheer, A., Zhu, L. (2012). Quantitative cone-beam CT imaging in radiation therapy using planning CT as a prior: First patient studies. Medical Physics, 39(4), 1991-2000.

Palombarini, M., Mengoli, S., Fantazzini, P. *et al*. (2012). Analysis of inter-fraction setup errors and organ motion by daily kilovoltage cone beam computed tomography in

intensity modulated radiotherapy of prostate cancer. Radiation Oncology, 7(1), 56. doi:10.1186/1748-717X-7-56.

Parham, A., George, D. (2010). Inclusion of the dose from kilovoltage cone beam CT in the radiation therapy treatment plans. Medical Physics, 37(1), 244-8.

Ploquin, N., & Dunscombe, P. (2009). A cost-outcome analysis of image-guided patient repositioning in the radiation treatment of cancer of the prostate. Radiotherapy and Oncology, 93(1), 25-31.

Pollack, A. (2011). RTOG 0534 protocol. Radiation Therapy Oncology Group clinical trials. Retrieved from http:// www.rtog.org/ClinicalTrials/ProtocolTable/StudyDetails.aspx?study=0534.

Richter, A., Hu, Q., Steglich, D. *et al*. (2008).Investigation of the usability of cone beam CT data sets for dose calculation. Radiation Oncology, 3(), 42. doi:10.1186/1748-717X-3-42.

Rong, Y., Smilowitz, J., Tewatia, D. *et al*. (2010). Dose calculation on kV cone beam CT images: an investigation of the Hu-density conversion stability and dose accuracy using the site-specific calibration. Medical Dosimetry, 35(3), 195-207.

Sandhu, A., Sethi, R., Rice, R. *et al*. (2008). Prostate bed localization with image-guided approach using on-board imaging: Reporting acute toxicity and implications for radiation therapy planning following prostatectomy. Radiotherapy and Oncology, 88(1), 20–5.

Schiffner, D. C., Schultheiss, T., Chen, Y. *et al.* (2012). Residual setup errors and dose variations with less-than-daily image guided patient setup in external beam radiotherapy for esophageal cancer. Radiotherapy Oncology, 102(2), 309-14.

Shannon, C. E. (1948). A mathematical theory of communication (part 1). The Bell System Technical Journal, 27, 379-423.

Shannon, C. E. (1948). A mathematical theory of communication (part 2). The Bell System Technical Journal, 27, 623-656.

Sheskin, D. (2004). Handbook of Parametric and Nonparametric Statistical Procedures (3rd Edition). Boca Raton: Chapman & Hall/CRC.

Snir, J. A., Battista, J. J., Bauman, G. *et al.* (2011). Evaluation of Inter-fraction Prostate Motion using Kilovoltage Cone Beam Computed Tomography during Radiotherapy. Clinical Oncology , 23(9), 625-31.

Sylvester, J. E., Grimm, P. D., Wong, J. *et al.* (2011). Fifteen-year biochemical relapse-free survival, cause-specific survival, and overall survival following I(125) prostate brachytherapy in clinically localized prostate cancer: Seattle experience. International Journal of Radiation Oncology, Biology and Physics, 81(2), 376–81.

Vivek, N. (2002). Prostate Cancer Diagnosis, staging and survival. Cancer Metastasis Reviews, 21(1), 17-27.

Wierzbicki, M., Schaly, B., Peters, T. *et al*. (2010). Automatic image guidance for prostate IMRT using low dose CBCT. Medical Physics, 37(7), 3677-86.

Yang, Y., Schreibmann, E., Tianfang, L. *et al*. (2007). Evaluation of on-board kV cone beam CT (CBCT)-based dose calculation. Physics in Medicine and Biology, 52(3) 685-705. doi:10.1088/0031-9155/52/3/011.

Appendix 1

This section contains a detailed list of the scripts used for the image registration method and for the cumulative dose calculations. Table A1.1 includes a short description of the Scripts.

Script	Action
Convert_OBI_DICOM_to_P3.py	Converts DICOM format images to P3 format.
Prep_CBCT.py	Aligns CBCT image isocenter with the isocenter selected for treatment in the planning CT image.
make_Mask.py	Generates the mask that limits the area of the images considered during image registration.
resample_Images.py	Resamples two images to a common voxel size.
pad_Image.py	Add zero-valued regions to images to obtain images with the same dimensions.
ImageGlobalRegistration_v11.py	Registers two images using a combination of rotations, translation, and scaling.
ImageDeformableRegistration_v12.py	Registers two images using a deformable transformation (vector field).
apply_XFM_to_Image.py	Applies a transformation to an image.
remove_Couch.py	Eliminates the CT couch from an image.
convert_Contours_to_Mask_Outline.py	Converts contours created for rectum and bladder into mask outlines.
fill_Edge_Image_Manual.py	Fills the mask outline manually with fixed intensity values. (used specifically to fill the bladder outline since is possible to find two outlines in the same slice)
fill_Edge_Images.py	Fills the mask outline automatically (used principally to fill rectum and rectal gas outlines).
binarize_Image.py	Assigns fixed intensity values to an image corresponding to the rectum and bladder.
convert_ROI_to_Poly.py	Converts a Pinnacle ROI structure into a VTK mesh file.

convert_Poly_to_Edge_Image.py	Converts a VTK mesh into a mask outline image
invert_Transform.py	Inverts a transform to calculate cumulative doses.
combine_Transform.py	Combines transformations into a single transform.
fix_Dose_Grid_Origin.py	Sets the origin for the dose grid to properly position it in the TPS.
sum_Dose_Grids.py	Sum dose grids from different fractions.

Table A1.1. Description of the Scripts**.**

Appendix 2

This section provides a data table (Table A2.1) with the alpha parameters that were used in every image registration. Alpha is a regularization parameter that restricts the magnitude of the deformation. Its purpose is to prevent extreme deformations. Three alphas were selected for every registration [α_1, α_2, α_3], pertaining to each of the three scales of the multi-resolution optimization approach.

Patient	Fraction	α_1	α_2	α_3
1	01	750.0	250.0	75.0
	02	200.0	1750.0	3000.0
	03	750.0	250.0	75.0
	04	200.0	1750.0	3000.0
	05	750.0	250.0	75.0
	06	750.0	250.0	75.0
	07	200.0	1750.0	3000.0
	08	200.0	1750.0	3000.0
	09	750.0	250.0	75.0
	10	1000.0	500.0	2500.0
2	01	750.0	125.0	75.0
	02	750.0	1000.0	150.0
	03	750.0	125.0	75.0
	04	750.0	125.0	75.0
	05	750.0	1000.0	100.0
	06	750.0	1000.0	750.0
	07	750.0	1000.0	200.0
	08	750.0	125.0	75.0
	09	750.0	1000.0	150.0
	10	750.0	125.0	75.0
3	01	250.0	50.0	1500.0

	02	250.0	50.0	1500.0
	03	200.0	1750.0.0	3000.0
	04	250.0	50.0	1500.0
	05	250.0	50.0	1500.0
	06	250.0	50.0	1500.0
	07	250.0	50.0	1500.0
	08	250.0	50.0	1500.0
	09	250.0	50.0	1500.0
	10	250.0	50.0	1500.0
	01	150.0	150.0	150.0
	02	150.0	150.0	150.0
	03	750.0	250.0	75.0
	04	750.0	250.0	75.0
4	05	750.0	250.0	75.0
	06	750.0	250.0	75.0
	07	750.0	250.0	75.0
	08	150.0	150.0	150.0
	09	750.0	250.0	75.0
	10	150.0	150.0	150.0
	01	750.0	1000.0	150.0
	02	750.0	1000.0	150.0
	03	750.0	1000.0	150.0
	04	750.0	1000.0	150.0
5	05	750.0	1000.0	150.0
	06	750.0	1000.0	150.0
	07	750.0	1000.0	150.0
	08	750.0	1000.0	150.0
	09	750.0	1000.0	150.0
	10	750.0	1000.0	150.0
	01	750.0	125.0	75.0
6	02	750.0	125.0	75.0
	03	750.0	125.0	75.0

	04	750.0	125.0	75.0
	05	750.0	125.0	75.0
	06	750.0	125.0	75.0
	07	750.0	125.0	75.0
	08	750.0	125.0	75.0
	09	750.0	125.0	75.0
	10	750.0	125.0	75.0

Table A2.1. Alphas parameter selected for every registration [α_1, α_2, α_3], pertaining to each of the three scales of the multi-resolution optimization approach.

Appendix 3

This Appendix provides the raw, patient-specific data collected during this work. The tables contain the doses obtained at the RTOG 0534 limits while the figures show the DVHs for each patient.

	Dose (cGy) delivered by the evaluated scenarios					
DVH Quantity	RTOG 0534 Objective	Plan	Non-IGRT	IGRT	Alt-IGRT	Auto-IGRT
CTV(D_{100})	6480	6430	6160	6390	6260	6400
RECT(D_{35})	6500	4617	4949	4344	4774	4053
RECT(D_{55})	4000	2710	3222	2806	3134	2674
BLAD*(D_{50})	6500	1707	1558	1825	1870	1888
BLAD^{i}*(D_{70})	4000	1373	1467	1462	1464	1456
L.FEM. (D_{10})	5000	4717	4647	4577	4632	4443
R.FEM. (D_{10})	5000	4725	4441	4611	4481	4614

Table A3.1. Dose (cGy) calculated for the RTOG 0534 objectives over the studied alternatives for patient 1.

	Dose (cGy) delivered by the evaluated scenarios					
DVH Quantity	RTOG 0534 Objective	Plan	Non-IGRT	IGRT	Alt-IGRT	Auto-IGRT
CTV(D_{100})	6480	6390	6220	6240	6230	6250
RECT(D_{35})	6500	5393	5700	5729	5722	5809
RECT(D_{55})	4000	3813	4737	4772	4794	4926
BLAD* (D_{50})	6500	3205	2857	2915	2852	2883
BLAD* (D_{70})	4000	1507	1602	1636	1576	1570
L.FEM. (D_{10})	5000	4391	4370	4347	4368	4339
R.FEM. (D_{10})	5000	4284	4236	4228	4233	4229

Table A3.2. Dose (cGy) calculated for the RTOG 0534 objectives over the studied alternatives for patient 2

	Dose (cGy) delivered by the evaluated scenarios					
DVH Quantity	RTOG 0534 Objective	Plan	Non-IGRT	IGRT	Alt-IGRT	Auto-IGRT
CTV(D_{100})	6480	6410	5640	5400	5560	5180
RECT(D_{35})	6500	5417	4430	4209	4405	3920
RECT(D_{55})	4000	3191	3023	2717	2993	2598
BLAD*(D_{50})	6500	3925	1925	1815	1875	1840
BLAD*(D_{70})	4000	2032	918	863	882	872
L.FEM. (D_{10})	5000	4352	4304	4295	4294	4289
R.FEM. (D_{10})	5000	4531	4329	4429	4359	4469

Table A3.3. Dose (cGy) calculated for the RTOG 0534 objectives over the studied alternatives for patient 3.

	Dose (cGy) delivered by the evaluated scenarios							
DVH Quantity	RTOG 0534 Objective	Plan	Non-IGRT	IGRT	Alt-IGRT	Auto-IGRT	IGRT-5mm	IGRT-8mm
CTV(D_{100})	6480	6330	6160	6280	6260	6330	6210	6280
RECT(D_{35})	6500	6177	5944	6121	6014	6168	5826	6055
RECT(D_{55})	4000	5664	5466	5684	5572	5744	5147	5675
BLAD* (D_{50})	6500	4233	4827	4920	4864	4794	2535	3922
BLAD* (D_{70})	4000	3089	3657	3838	3737	3735	1812	3019
L.FEM. (D_{10})	5000	5083	5296	5159	5198	5126	5025	4990
R.FEM. (D_{10})	5000	5020	4907	4957	4932	5005	4783	4553

Table A3.4. Dose (cGy) calculated for the RTOG 0534 objectives over the studied alternatives for patient 4.

	Dose (cGy) delivered by the evaluated scenarios					
DVH Quantity	RTOG 0534 Objective	Plan	Non-IGRT	IGRT	Alt-IGRT	Auto-IGRT
CTV(D_{100})	6480	6390	6390	6400	6380	6400
RECT(D_{35})	6500	5625	5727	5694	5826	5687
RECT(D_{55})	4000	3869	4615	4405	4609	4375
BLAD* (D_{50})	6500	484	774	952	821	852
BLAD* (D_{70})	4000	191	290	308	298	301
L.FEM. (D_{10})	5000	4717	4647	4577	4632	4443
R.FEM. (D_{10})	5000	4725	4441	4611	4481	4614

Table A3.5. Dose (cGy) calculated for the RTOG 0534 objectives over the studied alternatives for patient 5.

	Dose (cGy) delivered by the evaluated scenarios					
DVH Quantity	RTOG 0534 Objective	Plan	Non-IGRT	IGRT	Alt-IGRT	Auto-IGRT
CTV(D_{100})	6480	6390	6180	6220	6220	6240
RECT(D_{35})	6500	5556	5761	5656	5687	5660
RECT(D_{55})	4000	4188	4813	4566	4642	4574
BLAD* (D_{50})	6500	4932	4646	4695	4714	4637
BLAD* (D_{70})	4000	3403	3313	3328	3342	3259
L.FEM. (D_{10})	5000	4378	4294	4302	4282	4347
R.FEM. (D_{10})	5000	4465	4392	4395	4420	4325

Table A3.6. Dose (cGy) calculated for the RTOG 0534 objectives over the studied alternatives for patient 6.

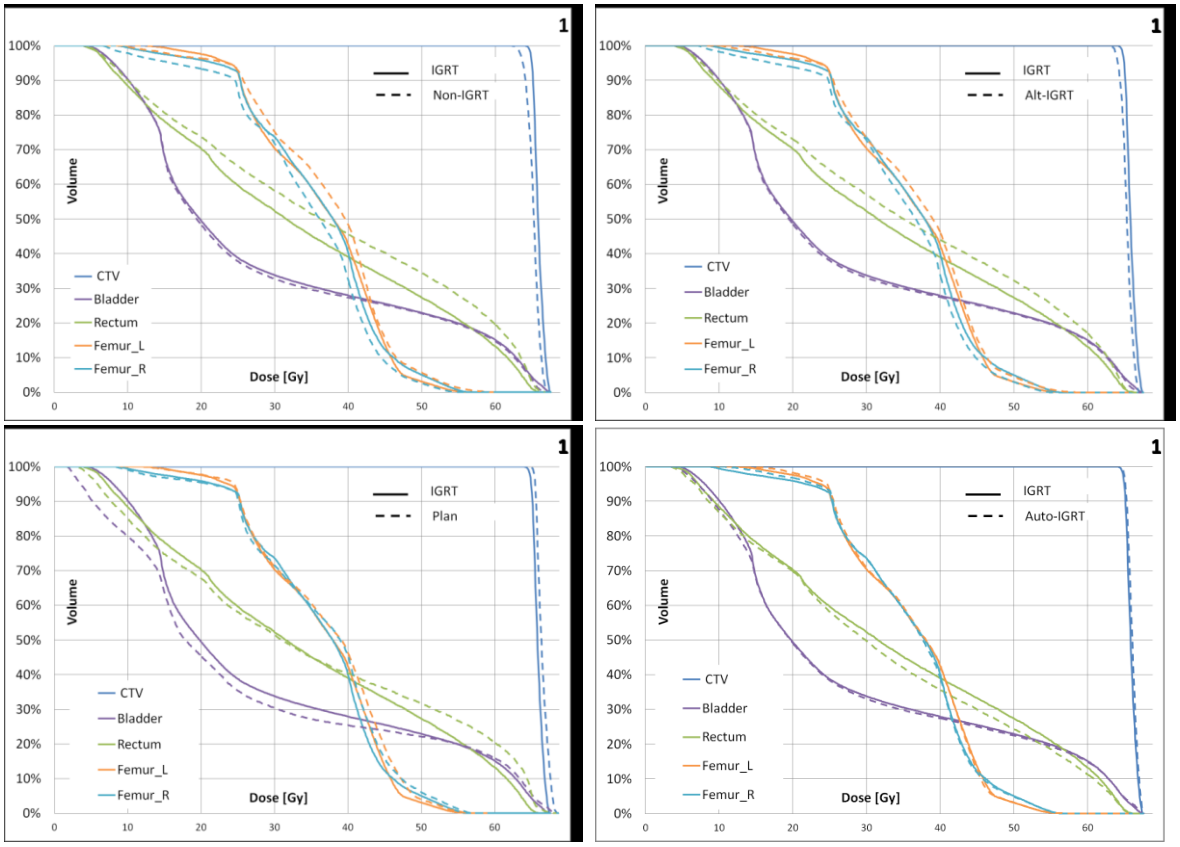

Figure A3.1. DVHs for the studied alternatives for patient 1.

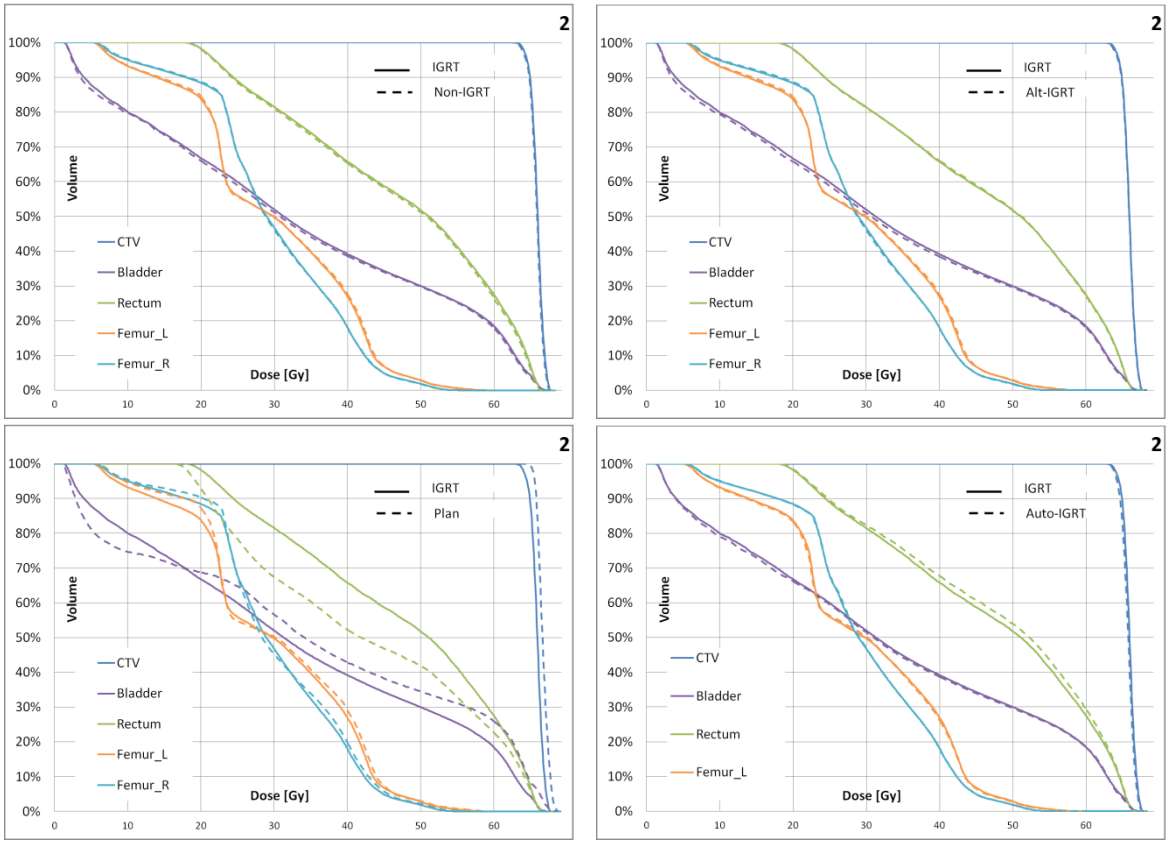

Figure A3.2. DVHs for the studied alternatives for patient 2

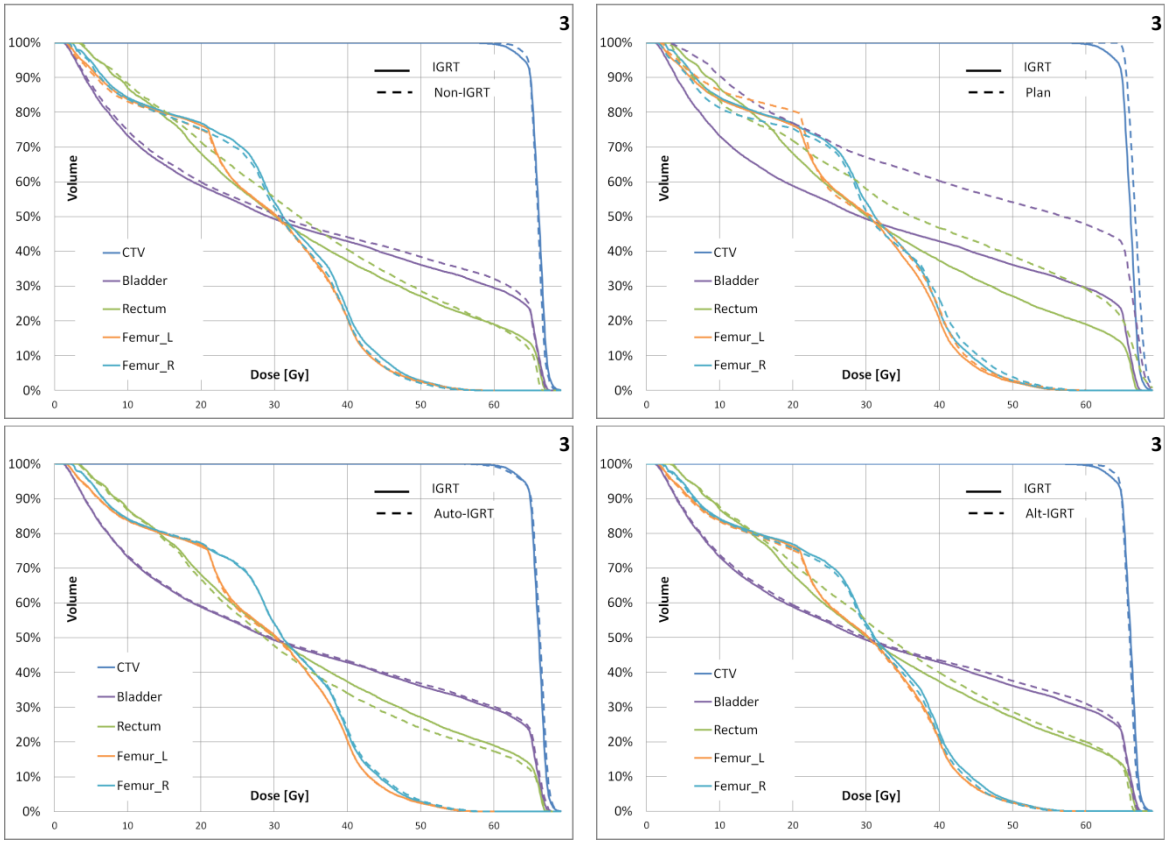

Figure A3.3. DVHs for the studied alternatives for patient 3

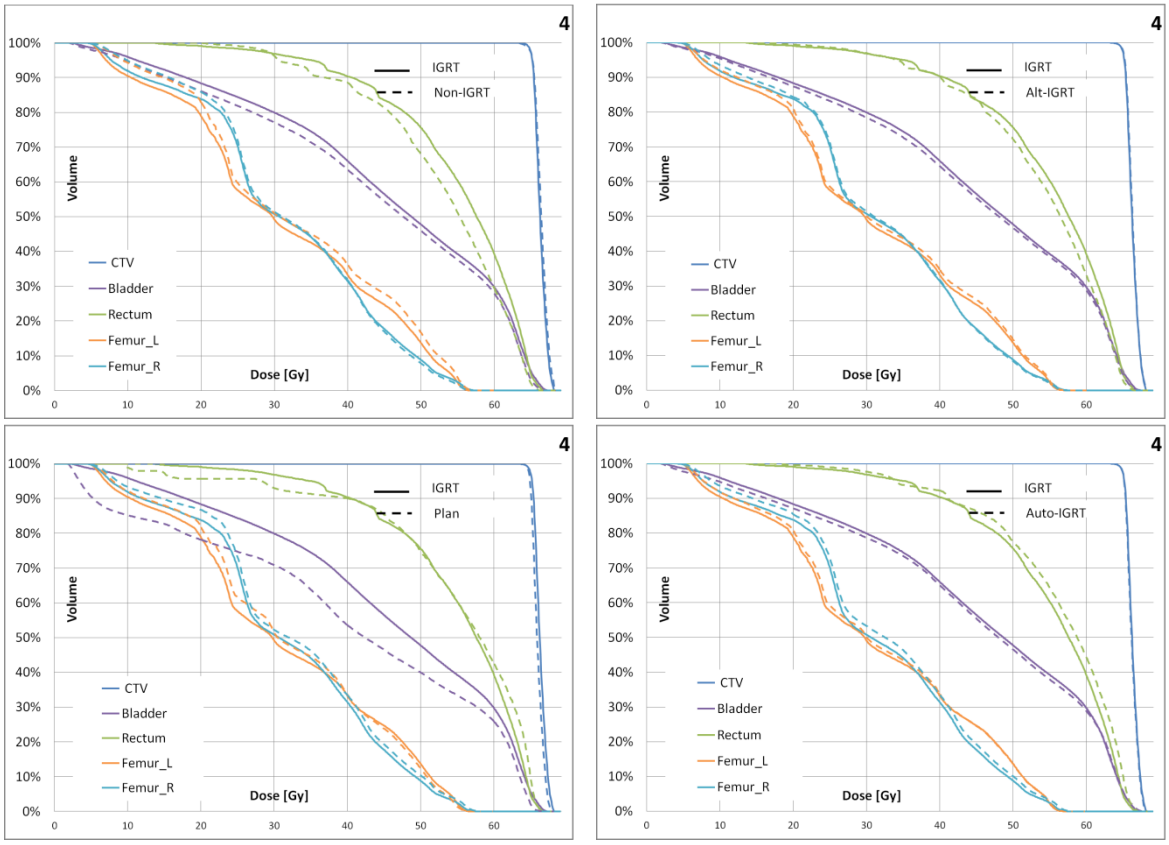

Figure A3.4. DVHs for the studied alternatives for patient 4

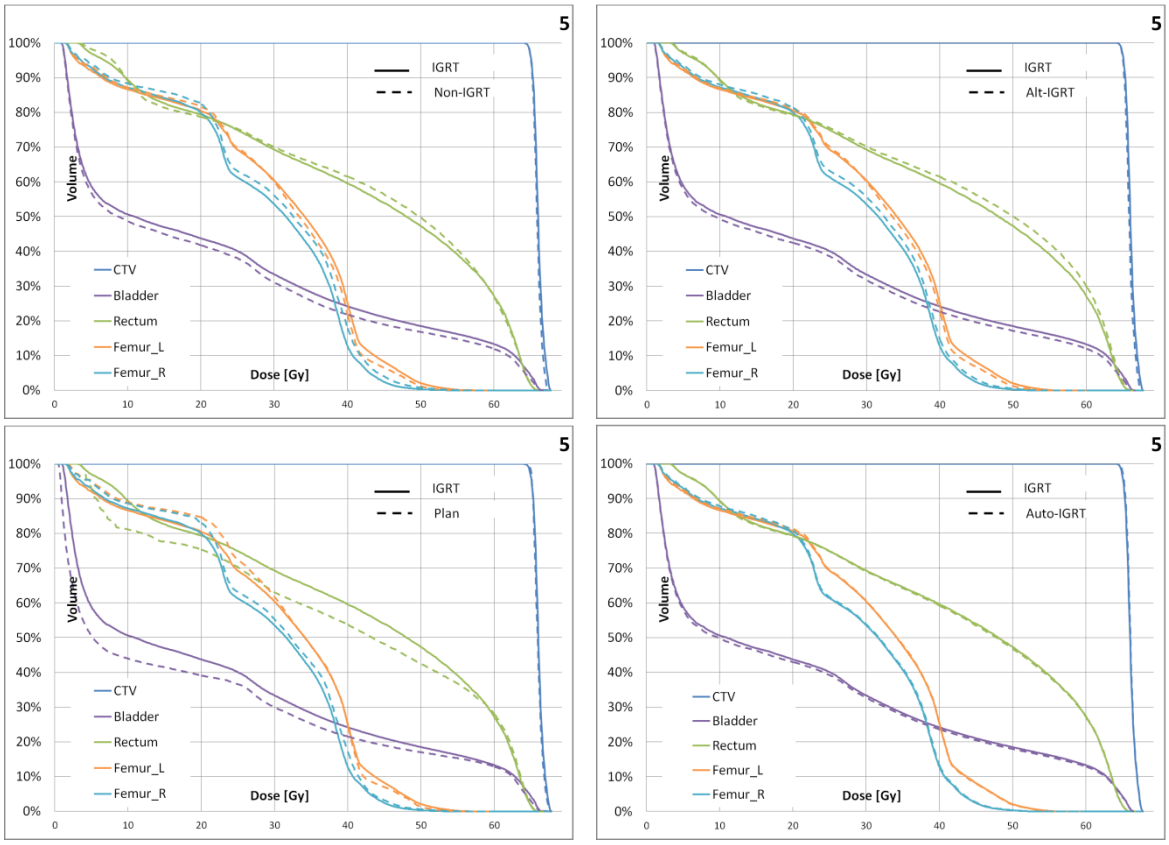

Figure A3.5. DVHs for the studied alternatives for patient 5

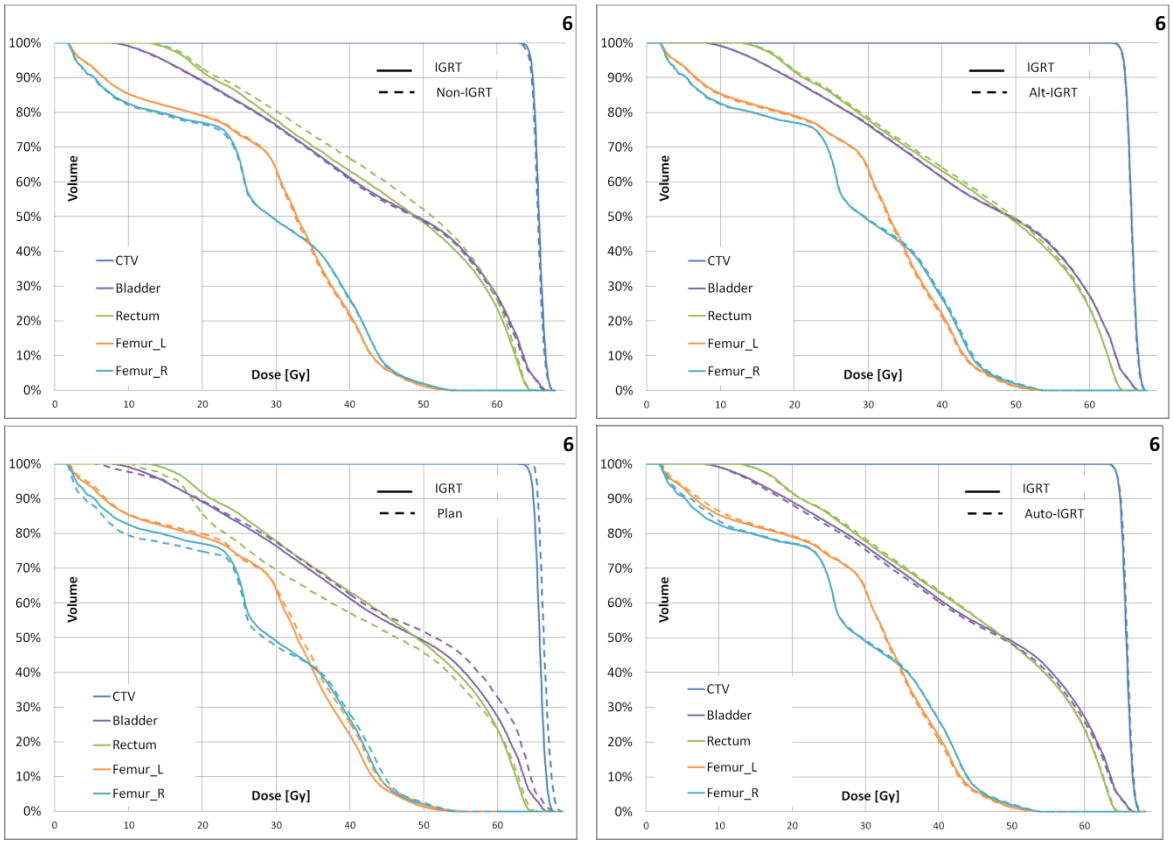

Figure A3.6. DVHs for the studied alternatives for patient 6

[i] BLAD* refers to bladder minus CTV